**PEOPLE'S DEMOCRATIC REPUBLIC OF ALGERIA**

**MINISTRY OF HIGHER EDUCATION AND SCIENTIFIC RESEARCH**

**IBN KHALDOUN UNIVERSITY OF TIARET.**

**FACULTY OF MATERIAL SCIENCES DEPARTMENT**

**OF PHYSICSDES SCIENCES**

# THESE

Prepared as part of an international thesis co-supervision with the University of Montpellier

Presented by:

M. MAHFOUD Mohamed

To obtain the diploma of:

Doctorat (L.M.D.)

Spécialité : **Materials Engineering**

Theme

# Study of nanomagnetic properties of multi functional nano - materials by an ultrasensitive planar Hal l effect microprobe

*At **15/12/2020** . :*

| | | | |
|---|---|---|---|
| M. BOUSSEKSOU Azzedine | DR | CNRS,LCC Toulouse | President |
| M.YAGOUBI Benabdellah | Pr. | University de Mostaganem | Examiner |
| M. EBOTHE Jean | Pr. | University de Reims | Examiner |
| M. MILOUA Redouane | Pr. | University de Tiaret | Examiner |
| M. BELARBI El Habib | Pr. | University de Tiaret | Director de These (Algeria) |
| Mme TERKI Férial | MC-HDR | University de Montpellier | Directrice de These (France) |
| M. BOUKRA Abdelaziz | MCA | University de Mostaganem | Co-supervisor (Algeria) |
| M. TRAN Quang Hung | MC-HDR | Ev-Technologies Caen | Co-supervisor (France) |
| M. SCALBERT Denis | DR | University de Montpellier | Invite |

**2020/2021**

الملخص

يؤدي تقليص حجم المواد المغناطيسية إلى المقياس النانوي إلى ظهور خصائص جديدة. على سبيل المثال ، تُظهر جسيمات الذهب النانوية خصائص مغناطيسية غير متوقعة يمكن التحكم فيها عن طريق التحكم في الحالة الكيميائية لسطحها. تعد هذه الخصائص بتقنيات ثورية. يتطلب تطوير هذه التقنيات فهما عميقا للتفاعلات بين الجزيئات وبين الجسيمات من خلال التوصيف الدقيق لكميات صغيرة من الجسيمات النانوية (ميكرو / نانوجرام). يمثل هذا الهدف تحديًا كبيرًا نظرًا لضعف دقة الأجهزة المستخدمة حاليا. تهدف هذه الأطروحة إلى تطوير مقياس مغناطيسي دقيق عالي الحساسية يتيح الكشف عن الخصائص المغناطيسية النانوية لكمية صغيرة من الجسيمات النانوية المعزولة. لذلك ، قمنا بدراسة كيفية تحسين الاستقرار الحراري للمستشعر المغناطيسي للحصول على قياسات دقيقة في بيئة درجة حرارة غير مستقرة من 5K إلى 410 K .تم ايضا فحص التفاعلات بين الجسيمات النانوية المغناطيسية والمستشعر المغناطيسي نظريًا لزيادة قدرة المستشعرعلى الكشف عن طريق تحسين هندسته. بناء على هذه التحسينات ، أثبتت تجريبياً ان مغناطيسية كميات متناهية الصغر من الجسميات النانوية الذهبية تعزز عن طريق ربط سطحها بمواد كميائية.

Résumé:

Les capteurs magnétorésistifs (MR) sont très intéressents dans de nombreuses applications, notamment les détections biologiques, les applications spatiales, les applications automobiles, les applications industriel, et la magnétométrie pour la caractérisation des nanomatériaux magnétiques. La clé importante des capteurs MR dans ces applications est la mesure des champs magnétiques locaux créés à partir d'objets magnétiques ou des courants électriques. Un capteur MR convertit le champ magnétique en une tension de sortie électrique afin d'être mesurée au moyen d'un voltmètre. Pour s'intéresser à ces applications émergentes, il faut des capteurs magnétiques à haut rendement aux propriétés uniques telles qu'une réponse électrique linéaire au champ magnétique, une sensibilité très élevée, une excellente reproductibilité, une faible limite de détection, des bruits faibles, une stabilité thermique élevée, et leur compatibilité avec la technologie des circuits intégrés (IC), et avec les systèmes de détection biologique miniatures.

Au cours des dernières décennies, les progrès de la fabrication des matériaux magnétiques de faible dimension accompagnés avec une compréhension approfondie des phénomènes spintroniques ont conduit à l'invention de plusieurs types de capteurs magnetoresistance, notamment le capteur à magnétorésistance géante (GMR) et le capteur à résistance de Hall planaire (PHR). Le capteur GMR modifie sa résistance par le filtrage des électrons en utilisant l’orientation relative de la magnétisation des couches des capteurs. En revanche, pour le capteur PHR sa résistance change en raison du changement de son aimantation. De manière intéressante, ces capteurs magnétorésistifs possèdent les caractéristiques requises pour les applications mentionnées ci-dessus, notamment en la nouvelle génération de biopuce, et en micromagnétométrie ultrasensible pour la caractérisation de micro et nanoobjets magnétique.

De plus, l'utilisation de capteurs à magnétorésistance pour la détection de nanoparticules magnétiques est une perspective prometteuse pour le développement des systèmes technologiques innovants pour la science fondamentale et appliquée. Par exemple, les propriétés inconnues du nanomagnétisme dans les nanoparticules d'or le rendent attractif pour de nouvelles applications. La possibilité d'activer et de contrôler le magnétisme provenant d'une nouvelle réorganisation des charges électriques sur les nanoparticules d'or via l'interaction entre leurs surfaces et des particules biologiques ou

polymères pourrait conduire à l'émergence de capteurs bio-magnétiques ultra-sensibles. Le développement de tels dispositifs nécessite une compréhension approfondie des interactions chimiques entre les surfaces des nanoparticule d'or et les molécules biologiques par la caractérisation des faibles quantités des nanoparticles. Les dispositifs conventionnels tels que le SQUID et le magnétomètre à échantillon vibrant (VSM) ne peuvent être utilisés que pour caractériser les propriétés magnétiques de grand volume d'échantillon de matériaux magnétiques, alors que les micro-SQUIDs pourraient caractériser les propriétés magnétiques à l'échelle nanométrique des matériaux avec la contrainte de fonctionnement à basse température ($T < 4K$). Par conséquent, le développement de nouveaux dispositifs de capteurs ultrasensibles consacrés à la détection de très petites quantités de nanoparticules de la température ambiante à des températures élevées est un sujet important pour amener les connaissances physiques des nanomatériaux à la frontière de la science.

Le capteur à effet Hall planaire est l'un des capteurs à magnétorésistance les plus prometteurs pour la caractérisation et la détection de petits échantillons de nanoparticules magnétiques. Au cours des deux dernières décennies, les améliorations des structures du capture Hall planaire [1-3] et des géométries [4,5] du capteur Hall planaire ont permis d'améliorer sa stabilité thermique, sa sensibilité au champ magnétique, et augmenté sa réponse électrique,. En comparaison avec d'autres capteurs à magnétorésistance, le capteur à effet Hall planaire a un rapport signal sur bruit élevé, une réponse linéaire à faible champ magnétique, de grandes surfaces actives qui est une caractéristique importante pour les applications biologiques, et une stabilité thermique élevée. A base de ces avantages, le capteur PHR a été utilisé dans de nombreuses applications biologiques pour la détection et la manipulation de molécules biologiques. Le principe de détection dans ces applications se base sur la détection du champ magnétique créé à partir de micro ou nanoparticules attachées sur des molécules biologiques. Ce principe de détection simple, en plus des caractéristiques distinctives du capteur, rend la bio-détection utilisant les capteurs à effet Hall planaires une acquisition flexible, facile et rapide. Le capteur Hall planaire a été utilisé pour étudier la cinétique d'hybridation de l'ADN [6], et pour mesurer la dénaturation de l'ADN sous l'effet de la température ou du sel [7]. En plus de ces applications biologiques, le capteur à effet Hall planaire peut être utiliser pour les applications industrielles telles que l'inspection des oléoducs et gazoducs [8], les applications automobiles et les applications spatiales notamment dans les nouvelle génération des nano ou picosatellite

Dans le domaine de la magnétométrie, le groupe de recherche de l'INSERM Montpellier, que j'ai joint pour mener ce travail, a mis au point un magnétomètre ultrasensible pour détecter pour la première fois l'hystérésis thermique d'une très petite quantité de matériaux de transition de spin à l'aide d'un capteur planaire Hall ultra-sensible [9,10] en collaboration avec le laboratoire de chimie de coordination, LCC Toulouse (France), et le laboratoire Nano Bio-Matériaux & Spintronique au DGIST (Daegu, Corée). Cette réalisation a ouvert la voie à l'utilisation de ce capteur magnétique comme un dispositif ultrasensible pour la caractérisation de petites quantités de nanoparticules à la température ambiante.

Dans cette thèse, je présente les détails d'investigation sur les capteurs à effet Hall planaires très sensibles pour pouvoir détecter et caractériser avec une haute précision de petites quantités de nanoparticules dans un environnement instable. Les résultats issus de cette thèse prouvent être rapidement appliquées à d'autres applications telles que les applications d'automobile, les applications 'industrie, les applications spatiales et les sciences de la vie.

Cette thèse est divisée en cinq chapitres:

Le chapitre 1 :

Je présente une étude complet des développements du capteur à effet Hall planaire, de la définition des concepts et les principes de base théoriques aux développements de la structure du capteur et des géométries du capteur. Ce chapitre fournit une connaissance de base pour comprendre les principes de fonctionnement du capteur.

Le chapitre 2 :

Je présente les procédés expérimentaux de la microfabrication du capteur en passant par la croissance du multicouche par pulvérisation cathodique à la conception et la réalisation de formes de capteur par technique de photolithographie.

Le chapitre 3

Je présent le détail des simulations théoriques des interactions magnétiques entre un capteur magnétique et des microparticules et nanoparticules magnétiques. La détection de microparticules et nanoparticules magnétiques par un capteur à effet de Hall planaire est essentiellement contrôler par la distribution du champ magnétique créé à partir de ces microparticules ou nanoparticules magnétiques sur la surface active du capteur Par conséquent, il est très important de comprendre la distribution de ces champs magnétiques.

Dans la première partie de ce chapitre, je présente une étude théorique de l'interaction entre des micro ou nanoparticules magnétiques et la surface du capteur en fonction de la taille des particules et de la taille du capteur. Je présente également l'étude du champ magnétique distribué créé à partir de micro ou nanoparticules magnétiques sur le capteur magnétique et la possibilité d'améliorer ce champ en optimisant la géométrie du capteur.

Dans la deuxième section de ce chapitre, je présente une étude théorique du champ magnétique traversant un capteur en forme de "ring" ainsi que la variation du moment magnétique des particules magnétisées par ce champ.

Afin d'augmenter la magnétisation des particules sans affecter leur stabilité thermique et celle du capteur, une nouvelle approche est proposée.

Le chapitre 4 :

Je focalise sur les comportements thermiques du capteur. En effet, la haute résolution du capteur est fortement dépendante de sa stabilité thermique, notamment pour la caractérisation des matériaux magnétiques, les applications biologiques et spatiales.

Dans la première section de ce chapitre, je présente une nouvelle méthode pour stabiliser la sensibilité du capteur lorsque la température passe de 110 K à 360 K en contrôlant l'interaction entre l'énergie Zeeman, l'énergie d'échange et l'énergie anisotrope du capteur. Cette méthode permet une stabilité thermique la plus élevée de la sensibilité du capteur par rapport aux autres capteurs MR tel que le capteur à magnétorésistance géante (GMR) ou le capteur à magnétorésistance à effet tunnel. De plus pour une compréhension approfondie de l'origine de la stabilité thermique du capteur, j'étudie la variation du champ d'échange, du champ de coercivité et de la résistivité anisotrope en fonction de la température. De plus, j'ai mis en évidence un petit changement de l'axe de facile aimantation de capteurs induit par le changement de température. La variation de l'énergie d'anisotropie en fonction de la température il a également été étudié

Dans la deuxième partie de ce chapitre, j'étudie la stabilité des capteurs dans des environnements thermiques tels que ceux imposés par les applications spatiales ou industrielles. J'étudie la variation de la tension PHR, le décalage de la tension du capteur, la sensibilité, la durabilité et le bruit thermique du capteur dans la plage de température entre -80 ° C jusqu'à 140 ° C. La transition de la magnétorésistance anisotrope de capteurs de l'anisotropie magnétique uniaxiale à l'anisotropie magnétique biaxiale sera mise en évidence dans cette section. La capacité du capteur à fonctionner très efficacement dans ces environnements thermiques difficiles a également été montrée.

Dans la dernière section de ce chapitre, j'étudie pour mettre en évidence que le capteur magnétique peut fonctionner à des températures extrêmement basses jusqu'à 5 K, le fonctionnement à cette basse température permet au capteur d'être utilisé dans des applications spatiales. Le comportement électromagnétique du capteur et la variation de sa sensibilité ont été étudiés.

Le chapitre 5 :

Je focalise sur la détection du «champ magnétique surprenant» récemment rapporté dans les nanoparticules d'or. Des quantités infinitésimales (2 microgrammes) de nanoparticules Au ayant différentes tailles et états ont été caractérisées a la température ambiant. Notamment, ces petites quantités de nanoparticules d'or ne peuvent pas être caractérisées à l'aide de dispositifs actuels de tels que SQUID, micro et nano SQUID. En effet, la sensibilité de notre configuration est de quatre fois magnitudes supérieures à celle du SQUID, ce qui permet de détecter une très faible aimantation c'est à dire ($10^{-14}$ emu) là où le SQUID conventionnel atteint ($10^{-7}$ emu en usage courant) et $10^{-10}$ emu donné par le constructeur en théorie.

Un des résultats préliminaires révèle clairement que le champ magnétique présent sur la nanoparticule d'or est amplifié par la fonctionnalisation. Ces premiers résultats sur des quantités aussi très faibles (2 microgrammes) semblent concorder avec une distribution de charges de surface due à la présence de fonctionnalisation polyéthylène glycol qui induisait la plus forte susceptibilité observée des nanoparticules d'or. Des mesures supplémentaires sur l'effet de taille et le type de fonctionnalisation doivent être réalisées pour progresser dans la compréhension du champ magnétique inattendu.

Mots de clé :

Nanomagnétisme, nanostructures, effet hall Planaire, anisotropie magnétique, Magnetoresistance, Capteurs magnétiques, susceptibilité magnétique.

Abstract:

The decrease in magnetic materials' size to the nanoscale leads to the emergence of new properties. For example, gold nanoparticles exhibit unexpected magnetic properties that could be manipulated by controlling the chemical state of gold nanoparticles' surface. These novel properties will open promising technologies, especially in industrial applications, biological detections, and data storage technologies. However, achieving these goals requires a deep understanding of the magnetic properties of small quantities of nanoparticles. Hitherto, the detection and the characterization of small amounts of nanoparticles have been a major challenge due to the limit of detection of the dedicated experimental magnetic conventional setup such as the conventional SQUID magnetometer ($10^{-7}$ emu) and the μ-SQUID low operating temperature (< 4K).

This thesis aims to develop a high sensitivity Planar Hall Effect sensor to be able to detect a small amount of nanoparticles. To achieve this objective, we studied first the interactions between the magnetic nano/microparticles and the sensor and the possibility of improving these interactions by optimizing the geometry of the sensor. Second, we improve the thermal stability of the sensor to be higher compared other magnetic sensors and allows extremely accurate measurements in unstable thermal environments ranging from 5K to 410K. Thirdly, we combine the theoretical studies on the interaction between the magnetic particles and the sensor and the high thermal stability of the sensor to characterize small samples of gold nanoparticles which cannot be detected by the current devices. These studies open the path for the sensor to be used in new applications such as the next generation of biological sensors, the nanosatellites' applications, and the most significant as an ultra-sensitive magnetometer in a wide temperature range 4K- 410K.

Keywords:

Nanomagnetism, nanostructures, Planar hall effect, magnetic anisotropy, Magnetoresistance, Magnetic sensors, magnetic susceptibility.

Acknowledgment:

First and foremost, praises and thanks to God, the Almighty, for His showers of blessings throughout my work to complete the research successfully.

I would like to express my sincere gratitude to my thesis supervisors, DR. Férial Terki, Pr. El Habib Belarbi, DR. Tran Quang Hung and, DR. Abdel Aziz Boukra for welcoming me warmly to their teams, their continuous support of my Ph.D study, their patience, motivation, enthusiasm, and immense knowledge.

I warmly thank our collaborators:

n-BEST laboratory of Professor CheolGi Kim in South Korea for the high quality of samples which allowed this work to be done.

Laboratory of Condensed Matter Chemistry Paris of Pr. Clement SANCHEZ for the high quality of the gold nanoparticles. Also, I warmly thank Pr. Azzedine BOUSSEKSOU who proposed this original study on the gold nanoparticles

I also thank Mrs. REZKALLAH Fatima for the administrative assistance that she provided throughout my PhD years.

I am extremely grateful to my mom for here love, prayers, caring and sacrifices for educating and preparing me for my future. I am very much thankful to my family for their love, understanding, prayers, and continuing support to complete this research work. Finally, my thanks go to my friends and research colleagues, and to all the people who have supported me to complete the research work directly or indirectly.

Mohamed MAHFOUD

Table of Contain

List of figures

List of tables:



Symbols and abbreviations:

| | |
|---|---|
| FM | Ferromagnetic. |
| AFM | Antiferromagnetic |
| AMR | Anisotropic Magnetoresistance |
| GMR | Giant Magnetoresistance |
| TMR | Tunneling magnetoresistance |
| PHR | Planar Hall Resistance |
| PHE | Planar Hall Effect |
| TCS | Temperature Coefficient of the sensitivity |
| SNR | Signal to noise ratio. |
| SOI | Spin orbital Interaction |
| *S* | Sensitivity |
| *R* | Radius |

## Motivation

Magnetoresistive (MR) sensors receive great interested in many applications including biological detections, space applications, automotive applications, and magnetometry for characterizations of magnetic nanomaterials. The important key of MR sensors in these applications is the measurement of magnetic field environment and the local magnetic fields created from magnetic objects or electrical currents. A MR sensor converted magnetic field into an electrical output voltage in order to be measured by means of a voltage meter. To be interested in these emerging applications, high-efficiency magnetic sensors with unique properties are required such as a linear electrical response to the magnetic field, a high sensitivity, excellent reproducibility, a low limit of detection, low noises, a high thermal stability, and their compatibility with Integrated Circuit (IC) technology and lab-on-a-chip devices.

In the past few decades, progress in manufacturing of low dimension magnetic materials accompanied by a deep understanding of spintronic phenomena led to the invention of several types of MR sensors including giant magnetoresistive (GMR) sensor and planar Hall resistance (PHR) sensor. GMR sensor changes its resistance by the filtering of electrons employing the relative orientation of the magnetization of the sensors' layers. On the other hand, a PHR sensor changes its resistance as a result of the change in its magnetization. Interestingly, these magnetoresistive sensors owning required characteristics for the above-mentioned applications, especially in next generation biochip, and in ultrasensitive micromagnetometry for characterization of micro and nanoobjects.

Moreover, the use of magnetoresistive sensors for detection of magnetic nanoparticles is a promising perspective for the development of innovative technological systems for both fundamental and applied science, especially in the developments and discoveries of physical insights of nanomaterials and molecules. For example, the unknown nanomagnetism properties in gold nanoparticles makes it attractive for new applications. The possibility of activating and controlling the magnetism originate from new reorganization of electrical charges on gold nanoparticles through the interaction between their surfaces and biological particles or polymer could lead to the emergence of Ultra-sensitive bio-magnetic sensors. The development of such devices requires a deep understanding of chemical surface interactions tuning nanomagnetism properties of gold nanoparticles by characterizing small sample volume. The conventional devices such as the Superconducting quantum interference device magnetometer (SQUID) and Vibrating sample magnetometer (VSM) can only be used to characterize magnetic properties

of large sample volume of magnetic materials, whereas the micro-SQUIDs could characterize magnetic properties at nanoscale of materials with the constraint of low temperature operation (T < 4K ). Consequently, the development of novel ultrasensitive sensor devices devoted to the detection of extremely small quantities of nanoparticles from room temperature to high temperatures is an important topic to bring physical insights of nanomaterials into frontier of science.

Planar Hall sensor is one of the most promising magnetoresistive sensors for characterization and detection of small samples of magnetic nanoparticles. In the last two decades, the improvements of planar Hall sensor's structures [1-3] and geometries [4, 5] allowed improvement of its thermal stability, and its magnetic field sensitivity. In comparison with other magnetoresistive sensors planar Hall sensor has a high signal-to-noise ratio, linear response at low magnetic field, large active surfaces and a high thermal stability. With these advantages, the PHR sensor has been used in many biological applications for the detection and the manipulation of biological molecules. The principle of detection in these applications is based on sensing the stray magnetic field created from micro or nanoparticles which are labelled onto biological molecules. This simple detection principle, in addition to the distinctive characteristics of the sensor makes the bio-detection using the planar Hall sensors flexible, easy and fast acquisition. Planar Hall sensor was used to study the hybridization kinetics of DNA [6], and to measure the DNA denaturation under the effect of temperature or salt [7]. In addition to biological applications, planar Hall sensor is convinced for industrial applications such as the inspection of oil and gas pipeline [8], automotive applications and the space applications.

In the magnetometer field, research group at PHYMEDEXP Montpellier, which I joint to conduct this work, initiated an ultrasensitive magnetometer to detect for the first time the thermal hysteresis of an ultra-small quantity of spin-crossover materials using an ultra-sensitive planar Hall sensor [9, 10] in collaboration with coordination chemistry laboratory, LCC Toulouse (France), and Nano Bio-Materials & Spintronics laboratory at DGIST (Daegu, Korea). This achievement paved the way for using a planar Hall magnetic sensor as an ultrasensitive device for characterization of small quantities of nanoparticles at room temperature.

In this thesis, I present the investigation details on highly sensitive planar Hall sensors to be able to detect and characterize accurately small quantities of nanoparticles in unstable temperature environments. The study in this thesis could be swift applied to other applications such as automotive, industrial, space applications and life science.

This thesis is divided into five chapters:

**Chapter 1** introduces a comprehensive review of the planar Hall sensor developments from the definition of concepts and the theoretical fundamentals to the developments of the sensor's structure and the sensor's geometries. This chapter provides a basis knowledge for understanding the principles of the sensor's operation.

**Chapter 2** presents the experimental microfabrication processes of the sensor from the growing of the multilayer by the sputtering to the design and realization of Planar Hall devices shapes by photolithography technique.

**Chapter 3** details theoretical simulations of the magnetic interactions between a magnetic sensor and magnetic micro and nanoparticles. The detection of magnetic micro and nanoparticles by a PHR sensor is basically governed by the distribution of the magnetic field created from these magnetic particles on the sensor's surface.

In the first section of this chapter, I present a theoretical study of the interaction between magnetic particles and the sensor surface as a function of size of the particle and the size of the sensor. I also present the study of the distributed magnetic field created from magnetic micro or nanoparticles on the magnetic sensor and the possibility of improving this field by optimizing the geometry of the sensor.

In the second section of this chapter, I present theoretical study of the magnetic field created by the biased current and the magnetic moment of magnetic particles magnetized by this field.

In addition, I propose a new approach to increase the magnetization of the magnetic particles without affecting the thermal stability of both the sensor and particles.

**Chapter 4** focuses on thermal behaviors of the sensor. Indeed, the high resolution of the sensor is strongly dependent on its thermal stability, especially for the characterization of magnetic materials, biological, and space applications.

In the first section of this chapter, I present a new method to stabilize the sensor sensitivity when temperature changes from 110 K to 360 K by controlling the interaction between Zeeman energy, exchange bias energy, and the anisotropic energy of the sensor. This method allows a highest thermal stability of the sensor's sensitivity compared to other MR sensors. Moreover for deep understanding of the origin of temperature stability of the sensor, I study the variation of exchange bias field, coercivity field and the anisotropic resistivity as a

function of the temperature. In addition, I evidenced a small change of the easy magnetization axis of the sensor stack induced by the change of the temperature.

In the second part of this chapter, I study sensor's stability in harsh thermal environments such as those imposed by space or industrial applications. I study the variation of PHR voltage, the offset, the sensitivity, the durability, and the thermal noise of the sensor in the range of temperature from -80 °C to 140 °C. Importantly, the transition of the anisotropic magnetoresistance of the sensor stack from uniaxial magnetic anisotropy to biaxial magnetic anisotropy will be highlighted in this section.

In the last section of this chapter, I study to evident that the magnetic sensor can perform at extreme low temperature down to 5 K, operation at this low temperature allows sensor for the use in space applications.

**Chapter 5** is devoted to the detection of "the surprising magnetic field" recently reported in gold nanoparticles. Infinitesimal quantities (2 microgrammes) of Au nanoparticles having different sizes and states were characterized. Notably, these small quantities of gold nanoparticles cannot be characterized using current state-of-the-art devices such as SQUID, micro and nano SQUID. Indeed, the sensitivity of our setup is 4 magnitude higher that the SQUID, which allows to detect very low magnetization *i.e* ($10^{-14}$ emu) where conventional SQUID reaches ($10^{-7}$ emu in current use) and $10^{-10}$ emu given by the constructor theoretically.

One important achievement from preliminary results clearly reveals that the magnetic field present on gold nanoparticle is magnified by the functionalization. These first results on such very low quantities (2 microgrammes) seems to agree with a surface charges distribution due to the presence of Polyethylene Glycol functionalization which induced the observed highest susceptibility of gold nanoparticles. Further measurements on size effect and type of functionalization must be achieved to progress in the understanding of the unexpected magnetic field.

# 1. Over view on planar Hall sensor

## 1.1 Introduction

From the smartphone [11] to the satellite [12] and throughout the electronic [13] and bio-electronic devices [14], the magnetoresistive sensors today are a key parameter in different technology applications due to their high efficiency, and low cost compared to other devices. The development of these sensors was based on the deep understanding of physical phenomena that emerging by the interaction between the charge of the electron and the magnetization of the magnetic material (for example AMR, anisotropy magnetoresistance) or the interaction between the charge and the spin of the electron (for example giant magnetoresistance). The magnetoresistance sensors could be divided into two global families. First, the magnetoresistance sensors where the sensing is based on the intrinsic magnetoresistance of the ferromagnetic materials (such as anisotropic magnetoresistance AMR sensor or the planar Hall Effect sensor). Second, the magnetoresistance sensor where the sensing is based on the filtrate of electrons in the magnetic multilayers based on the quantum Pauli Exclusion Principle (such as the GMR giant magnetoresistance or the TMR Tunneling magnetoresistance sensor). Both families have a deep involvement in modern technologies. The AMR sensor, for example, was largely used in the early nineties as a read head in the computers [15] and it's used recently in the biochips [16] and automotive applications [17] due to its ability to detect a low magnetic field. The AMR was replaced by the GMR sensor in the read-head applications [18].

In this chapter, we will focus on the planar Hall magnetoresistive sensor which was recently developed compared to other magnetoresistive sensors (AMR, GMR, and TMR). We will draw the overall picture of the Planar Hall magnetoresistive sensor from the theoretical background to the development of the structure and the architecture. This chapter divided into four sections, the first section concerns the theoretical fundamentals of the planar Hall effect. In the second section, the development of the sensor stacks will introduce. The different structures of the sensor such as bilayer, spin valve, and the trilayer will be presented. The third section is dedicated to present the development of the shape of the sensor from the cross conventional shape to the elliptical shape. Other optimization of the sensor such as the increase of the sensitivity by changing the angle between the external magnetic field and the direction of the current will present in section four.

## 1.2 Theoretical background of the magnetic anisotropy and Planar Hall effect

When the physical properties of a material depend on the direction, this property is called anisotropy. In the same context, the anisotropic magnetoresistance is the dependence of the resistance of a material on its direction of magnetization. The phenomenon of the anisotropy magnetoresistance is discovered by William Thomson (Lord Kelvin later on) in 1857. In his paper titled "Effects of Magnetization on the Electric Conductivity of Nickel and of Iron"[19], William Thomson observes a change in the resistance of iron under the effect of an external magnetic field. The physical explanation of this phenomenon was delayed for more than a century as a result of the impossibility to explain it using classical physical concepts. Based on Smith's paper in 1951[20], the anisotropic magnetoresistance in ferromagnetic materials was explained using the two current model of conduction in transition metals (1936) [21]. This model was developed by Sir N.F Mott in order to explain the behavior of the resistivity of the nickel at a lower temperature than the temperature of Curie ($T < T_c$). The model deals with the electrons carrying the current in the transition metal materials as two electric currents. The first current is the one created by the spin up, and the second current is the one created by the spin down. Furthermore, the model supposes that the state of the electrons is conserved in the scattering processes. Several works in the 1960s and 1970s were dealt with electrical transport of the ferromagnetic materials based on Smith's work. These works are summarized in the famous review article published by McGuire and Potter in 1975 under the title "Anisotropic magnetoresistance in ferromagnetic 3d alloys"[22].

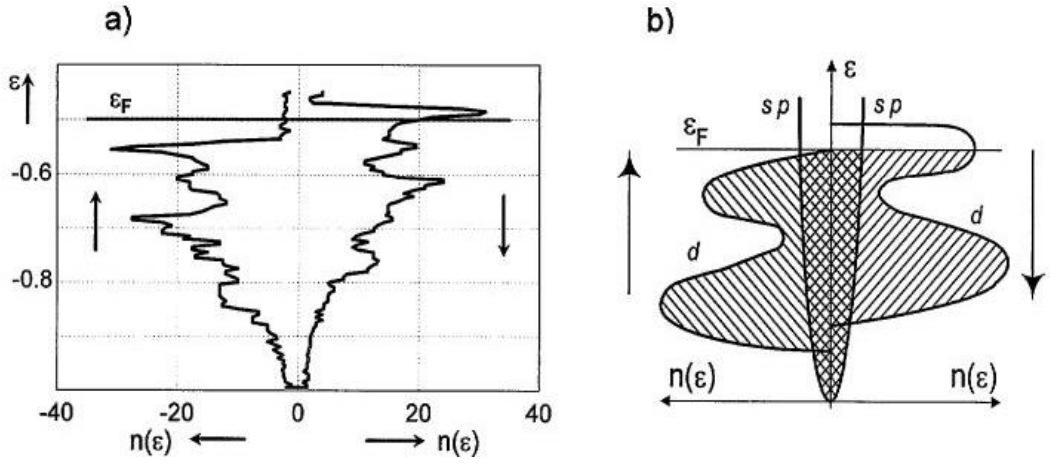


Figure 0.1 the density of states of the Nickel ferromagnetic determined by Langlinais and Callaway (1972). [23]

In fact, the anisotropic magnetoresistance is related to different phenomena that appear in magnetic materials and are absent in other materials (nonmagnetic materials). In the ferromagnetic materials such as the Ni, the energy band of electrons split into two different sub-

bands representing the two orientations of the spin up and down (see FIG. 1.1). Usually, in the ferromagnetic materials, the density of states of the spin-up electrons is different from that of the spin-down electrons.

Moreover, the 3d electronic band in some ferromagnetic materials, Ni for example, is not fulfilled. This leads to the scattering of the conduction electron from the 4s states to the 3d states. The scattering of the electrons to the 3d increases the resistivity of the ferromagnetic materials due to the high effective mass of the 3d electrons (high effective mass induces low conductivity of the electrons). In some ferromagnetic materials, the $3d^+$ non-occupied density of states of the spin up is bigger than the $3d^-$ non-occupied density of states of the spin down. Based on the Pauli Exclusion Principle "No two identical fermions may occupy the same quantum state", the probability of the 4s+ scattering to the $3d^+$ states is higher than the $4s^-$ scattering to the $3d^-$ (See FIG. 1.2)

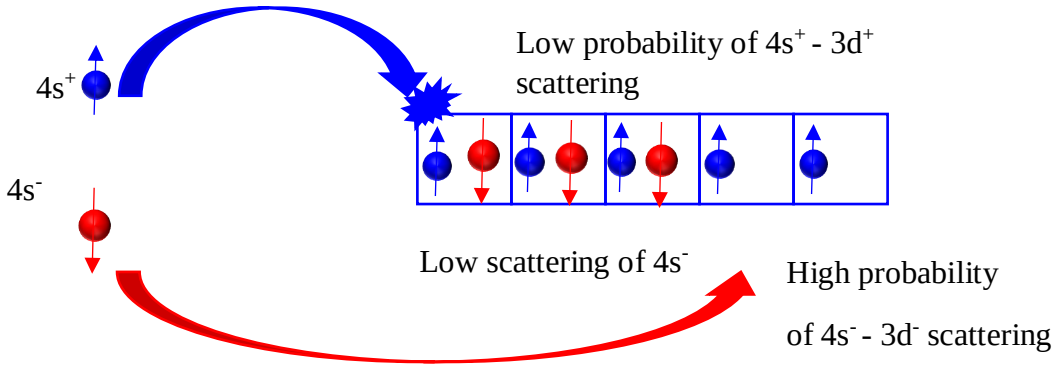


Figure 1.2 The Two current model propose by Mott

The high probability of the scattering of the $4s^+$ induces a high resistivity of these electrons due to the high effective mass in the $3d^+$ states. Meanwhile, the low probability of the scattering of the $4s^-$ electrons to the $3d^-$ states induces a high conductivity of these electrons. The resistivity of the material is the average of both the spin up and the spin down resistivities. In addition, because the spin up electrons have a high density, the metal tends to take electrical conductor behavior. Some other ferromagnetic materials have an inverse behavior where the scattering of the $4s^-$ electrons to the 3d- states is more probable than the scattering of the 4s+ to $3d^+$. For the Ni (nickel) only scattering from the $4s^-$ state to the $3d^-$ state is probable, due to the existence of the 3d+ sub-band below the Fermi level (See FIG.1.2).

However, the behavior of the electrons in the transition metal changes totally under the effect of an external magnetic field. The magnetic field induces the rotation of the magnetization from the easy axis (the axis that the magnetization prefers to orientate in its direction when the applied field is nil) to the direction of the external magnetic field. Smith related the anisotropy magnetoresistance which appears when the magnetization direction change to the mixing of the $d^+$ and $d^-$ states due to external magnetic field influence and the spin-orbital interaction [20]. This mixing leads to increasing the s-d scattering probability of the electrons traveling parallel to the magnetization. Consequently, the resistivity parallel to the magnetization is larger than the resistivity perpendicular to the magnetization; therefore, the anisotropy magnetoresistance appear. The FIG. 1.3 shows the variation of the resistivity of NiCo alloy as a function of the magnetic field induction. The longitudinal resistivity of the magnetic material is clearly larger than the transversal resistivity of the magnetic material. The difference between these two resistivities $(\rho_{//} - \rho_{\perp})$ is an important parameter to show how much a magnetic material has anisotropy, this parameter called the anisotropic resistivity.

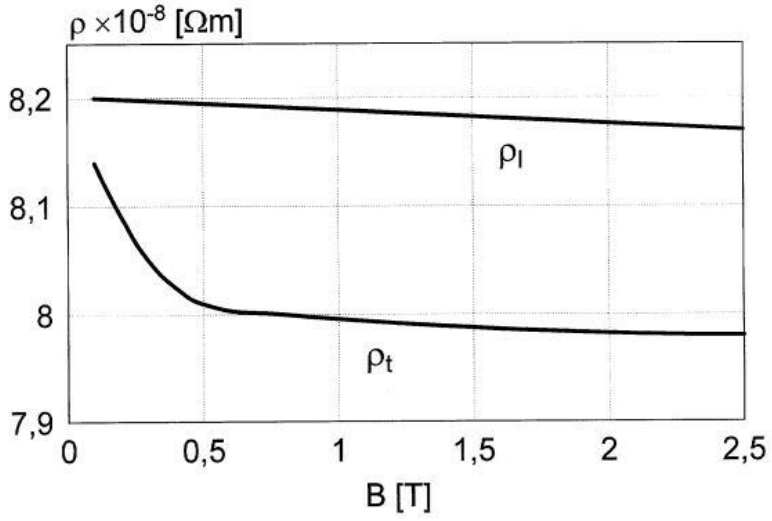


Figure0.3 The change of resistivity of NiCo alloy versus the external magnetic induction (McGuire and Potter 1975) [22]

The anisotropic magnetoresistance induces the change in the resistivity of the ferromagnetic material. The perpendicular variation of the resistivity to the easy axis is called the Planar Hall Effect and the parallel variation of the resistivity to the easy axis is called the anisotropic magnetoresistance. The Planar Hall Phenomenon was described by C. Goldberg and E. Davis in 1954 [24]. The name Planar comes from the fact that this phenomenon is induced from the change in the plan magnetization of the thin films. However, in the case of Ordinary Hall Effect which due to the Lorentz force, the creation of a transverse voltage is

induced by an external magnetic field applied perpendicularly (out plan) to the thin film, hence we use the name "Planar".

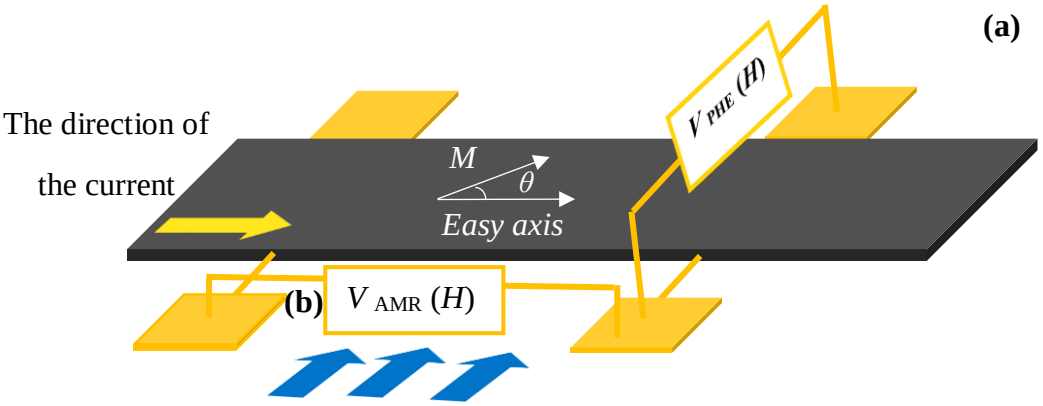


Figure 1.4 The Planar Hall Effect and, the anisotropic magnetoresistance effect induced by the change of the magnetization of a ferromagnetic material from the easy axis direction (which is parallel to the direction of the current) to the direction of applied field

Using Ohm law, the relation between the electrical field and the resistivity in the case of an anisotropic material give as:

$$\vec{E} = \vec{\rho}\,\vec{J} \qquad (1.1)$$

Where $\vec{E}$ is the electrical field, $\rho$ the resistivity of the material and $\vec{J}$ is the electrical density of the current.

The resistivity of the material is given by:

$$\begin{bmatrix} \rho_{\perp}(H) & -\rho_H(H) & 0 \\ \rho_H(H) & \rho_{\perp}(H) & 0 \\ 0 & 0 & \rho_{//}(H) \end{bmatrix}$$

Where $\rho_{\perp}$ is the resistivity of the material perpendicular to the magnetization, $\rho_{//}$ is the resistivity of the material parallel to the magnetization and $\rho_H(H)$ is the Hall resistivity.

When the magnetization makes an angle $\theta$ with the current direction (the easy axis direction), both Planar Hall voltage and the anisotropic magnetoresistance voltage are given by:

$$E_x = j\,\rho_{\perp} + j\,(\rho_{//} - \rho_{\perp})cos^2(\theta) \qquad (1.2)$$

$$E_y = j\,(\rho_{//} - \rho_{\perp})\cos(\theta)\sin(\theta) \qquad (1.3)$$

The transversal voltage is called the Planar Hall Effect or pseudo Hall Effect and the longitudinal compound is called the anisotropic magnetoresistance. From the expression above the Planar Hall effect is basically an anisotropy magnetoresistance effect.

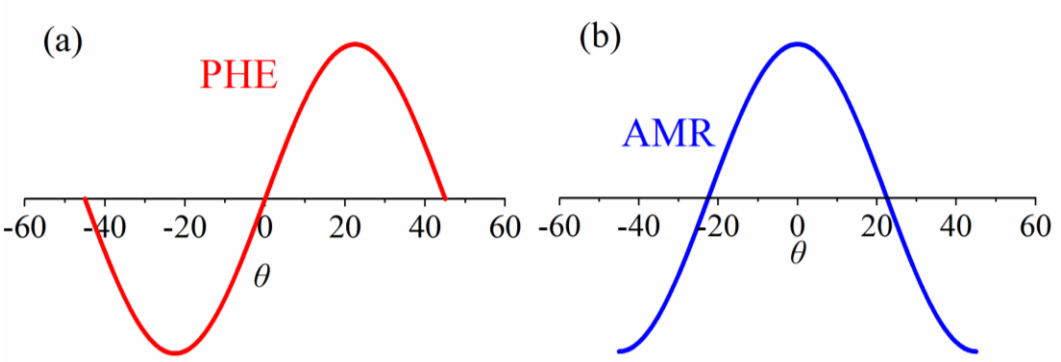


Figure 0.5 The variation of the planar Hall voltage and (b) the anisotropic magnetoresistance voltage both versus the angle between the magnetization and the direction of the current (θ).

The figure 1.5 shows the variation of the planar Hall voltage and the anisotropic magnetoresistance voltage as a function of the angle $\theta$ (The angle between the magnetization and the current direction). The Planar Hall voltage shows a linear dependence on the angle $\theta$ when the angle is small. This means that the electrical response of the planar Hall sensor is linear when we applied a small external magnetic field which is an important feature in the application of the sensor to detect ultra-low magnetic fields. Furthermore, from the equation (1.1) of the planar Hall voltage, the voltage depends only on the difference between the parallel and the perpendicular resistivity. This dependence makes the sensor more stable under the effect of the temperature compared to the anisotropic magnetoresistance sensors. These features and other features make the planar Hall sensor a promising device for detecting small magnetic fields with high accuracy.

## 1.3 The Development of the Sensor's Stack

The pioneering paper published by A. Schuhl et all opened the way to the use of the Planar Hall effect as a magnetic field sensor [25]. In their research paper under the title "Low Field Magnetic Sensors Based on the Planar Hall Effect", A. Schuhl and his colleagues used an ultra-thin layer of Permalloy (6 nm) coupled to a Fe ferromagnetic layer as a magnetoresistance sensor able to detect an ultra-low magnetic field. The choice of the Permalloy is based on the fact that its anisotropy resistivity is bigger than the transition metals such as Fe or Ni [22]. The sensitive layer of this sensor shows a magnetoresistance ration of 2% and an ultra-high sensitivity of 100V/TA. The second generation of the Planar Hall magnetoresistance sensor was

fabricated using the conventional sputtering system, where the Permalloy layer growth directly on silicon substrates [26]. The low-cost fabrications method (sputtering) proposed in this paper promoted the use of the Planar Hall sensor in the academic field and facilitated the industrial production processes of the sensor. Following these works, several optimizations of Planar Hall sensors were proposed based on the development of the structure of the sensor. A Trilayer structure based on two ferromagnetic layers exchanging with an antiferromagnetic layer was fabricated by L. Ejsin et al to test the ability to use the Planar Hall sensor in biological detection [27]. Using this structure, the authors proved the ability to detect two types of magnetic beads the first is the micro-magnetic beads (2 µm) and the second is the nano-magnetic beads (250 nm). The authors demonstrated also the possibility of detecting a single micromagnetic bead (2 µm) by applying a current of 10 mA and under the effect an external magnetic field of 1.5 mT. This achievement leading to the use of the planar Hall sensor as a biological sensor for the first time. Compared to the other magnetoresistive sensor the planar Hall sensor has important advantages in the field of biological detection such as the high signal-to-noise ration and the large size of the active area uses for sensing.

### 1.3.1 The Bilayer Structure (Ferromagnetic/ Antiferromagnetic Layers)

In the middle of the last decade, the bilayer structure based on the ferromagnetic layer coupled with an antiferromagnetic layer was an excellent choice for the manufacture of Planar Hall sensors. In the FM structures the planar Hall voltage shows a non-reversal behavior. As shows in the FIG. 1.6 (b) the magnetization angle of a single ferromagnetic layer change from 0° to 90° when the field increase and from 90° to 180° when the magnetic field decrease. However, for the FM/AFM structure the magnetization angle of the ferromagnetic layer rotates from 0° to 90° when the field increase and from 90° to 0° when the magnetic field decrease due to unidirectional anisotropy. Also the hysteresis of the planar Hall voltage reduce due to the coherent rotation of the magnetization in the FM/AFM structure. This coherent rotation decreases also the Barkhausen noise and improves the thermal stability of the structure. The most used bilayer structure is the NiFe/IrMn structure due to the high anisotropy magnetoresistance of the NiFe, the high resistivity of the IrMn (which pushes the electrons to pass through the sensitive layer of the sensor (NiFe) and resulting in an increment of the sensor sensitivity and a decrement of shunt current), and the high Néel temperature of IrMn.

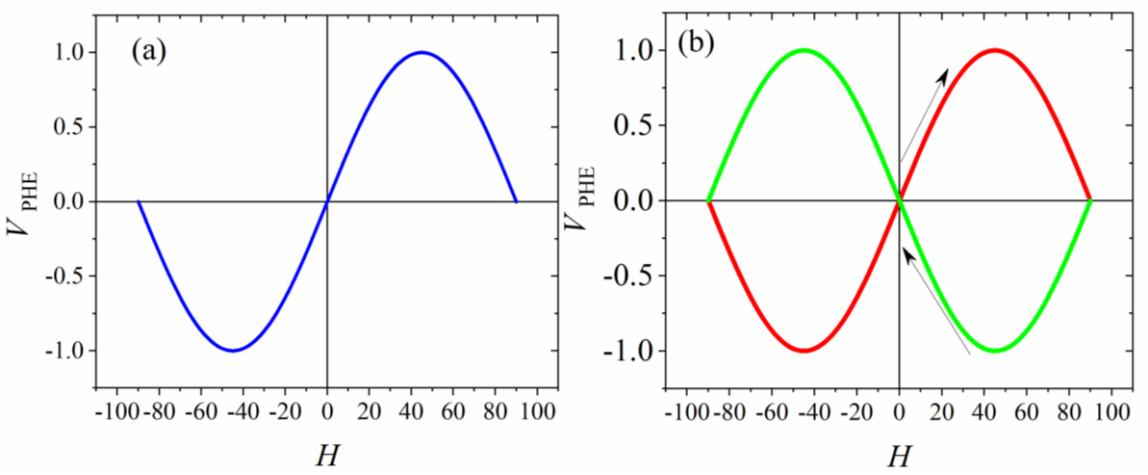


Figure 1.6 The calculated planar Hall voltage for (a) single ferromagnetic layer and (b) for exchange biased ferromagnetic/ antiferromagnetic layer.

To understand the effect of the ferromagnetic layer's size on the sensitivity of the sensor, a Planar Hall magnetoresistive sensor based on a bilayer structure was manufactured by the group of Pr. Kim in Korea. [1]. By changing the thickness of the ferromagnetic layer from 3 nm to 20 nm, they found that the sensitivity of the sensor increases with the increase of the ferromagnetic layer's thickness. However, the difference between the resistivity parallel to the magnetization and the resistivity perpendicular to the magnetization decreases when the ferromagnetic thickness is bigger than 10 nm. In addition, by using the Stoner-Wohlfarth model, the authors studied the dependence of the ferromagnetic thickness versus the exchange bias, anisotropy field, and the anisotropic resistivity. The study does not only demonstrate the possibility of an increased sensitivity of the sensor by increasing the thickness of the layer, but also demonstrates the possibility of using the Planar Hall effect to study the magnetic properties of a small magnetic stack which is difficult to study by using the conventional method. The same group studied the effect of the permalloy's (ferromagnetic layer which is also the sensitive layer of the sensor) thickness in bilayer structure on the amplitude of the PHE and AMR voltages. The study proves that the Ta and IrMn surface effect is dominated maximally by using a 10 nm NiFe layer that reflects in the high amplitude of both PHE and AMR voltage [28]. Also, the effect of the thickness of the sensitive layer (Permalloy) on the sensitivity of the Planar Hall sensor was studied by the group of Pr. Hansen [29]. The study proves that the high increase of the sensitive layer induces an increase in the signal and decrease the noise. In the following years, the use of trilayer and the spin valve structures dominated the use of the bilayer structure in the fabrication of the planar Hall sensors due to the high sensitivity and the high thermal stability of these layers.

### 1.3.2 The Spin Valve Structure

Despite the absence of a clear relationship between the spin-valve effect and the Planar Hall voltage, the spin valve structure which is based on two ferromagnetic layers separated by the non-magnetic layer (normally Cu) was widely used at the end of the last decade as a planar Hall sensor. The planar Hall voltage created in this spin valve structure is the result of the average contribution of the two ferromagnetic layers. The Planar Hall sensor based on the spin-valve structure was usually created on NiFe/Cu/NiFe/IrMn structure. Many papers were published at the end of the last decade which studied the planar Hall sensors based on spin valve structure among them. The work of S.J. Oh et al which focused on the effect of the size of the junction on the sensitivity of the Planar Hall sensor based on NiFe (6 nm)/ Cu (1.5 nm) / NiFe (4 nm) / IrMn (20 nm) [2]. This work proves that the sensitivity of the sensor decreases as its size increases. The same group uses a spin valve structure based on NiFe (6 nm)/ Cu (3.5 nm) / NiFe (3nm) / IrMn (10 nm) to detect a micro-magnetic bead for biological detection [30]. On the other hand, the effect of the size of the free ferromagnetic layer on the sensitivity of the Planar Hall sensor was studied by Hung et al [31]. They found that the sensitivity of the sensor increases as the thickness of the free layer increase. For a layer thickness of 16 nm, they obtained a sensitivity of 95.5 mΩ/(KA/m). Based on this optimization, Hung and his colleagues succeeded in detecting of a single micro-magnetic bead using Planar Hall sensor with a spin valve structure NiFe (16 nm)/ Cu (1.2 nm)/NiFe (2 nm)/IrMn (15 nm). [32]. Other layers were studied based on different materials such as Co/Cu/Py [3], and NiFer/CoFe/Cu/CoFe/IrMn [33]. However, the sensitivity of these structures is lower than the spin valve structure based on NiFe/Cu/NiFe/IrMn. Early this decade, the development of the spin valve structure for Planar Hall sensor was dominated by the development of new ultra-high sensitive trilayer structure which is the trilayer structure.

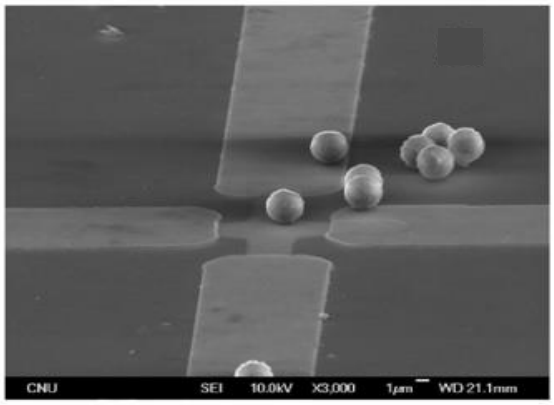


Figure 1.7 The SEM image of the planar Hall sensor in the presence of a single micro-magnetic bead [32].

### 1.3.3 Trilayer structure:

By using a very thin nonmagnetic layer placed between the ferromagnetic and the antiferromagnetic layers, Hung et al optimized seven times the bilayer structure sensitivity. Also, the sensitivity of this new structure which is known as the name of "the trilayer structure" is two times bigger than the spin valve structure [34]. The thickness of the nonmagnetic layer was optimized by studying the effect of different sizes of Cu layer on the sensitivity of the sensor [35]. Currently, this structure is the cornerstone of the development of high sensitivity Planar Hall sensors.

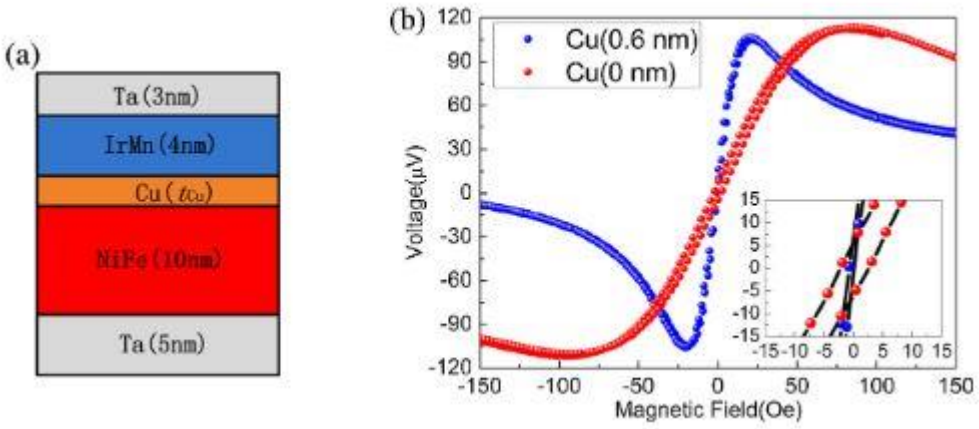


Figure 0.8 The Planar Hall voltage created by bilayer, spin valve and trilayer structures. [35]

The influence of Cu interlayer in the NiFe/IrMn interface on the rotation of the magnetic moments of the ferromagnetic layer was studied by Z-D. Zhao [36]. They prove in this paper that the existence of the ultra-small Cu interlayer reduces the hysteresis of the Planar Hall voltage which reflects the coherent rotation of the magnetic moments in the ferromagnetic layer (see FIG. 1.9).

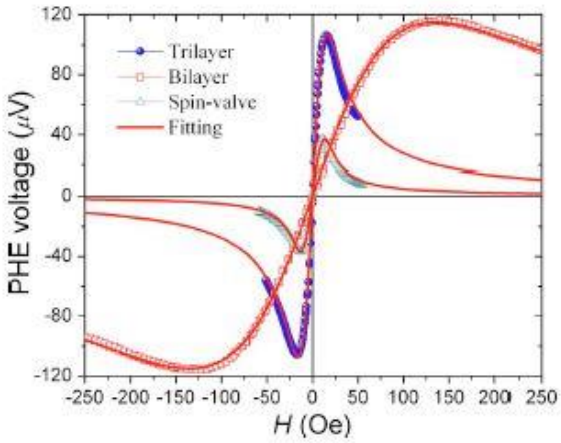


Figure 1.9 The planar Hall voltage created by trilayer structure (bleu curve) and the bilayer structure (red curve) [36]

In the same year, X-J Li, et al enhanced the sensitivity of the trilayer structure and its thermal stability using Au interlayer between the ferromagnetic and the antiferromagnetic layers. By studying the effect of the thickness of the Au layer on the planar Hall voltage, they proved that a trilayer of NiFe (10 nm) / Au (0.6 nm) / IrMn (10 nm) combines the high sensitivity, the coherent rotation of magnetization and the high thermal stability of the sensor [37]. Previous studies shows that the seed and the capped layer can affect the magnetic properties of the permalloy [38, 39], A Talantsev et al studied the effect of the NiFeCr seed and capping layers on both exchange bias and Planar Hall electrical response in NiFe/Au/IrMn layers [40]. The study is based on the change of the conventional Ta seed and capping layer which could format a dead magnetic layer by NiFeCr layers. The study proves that the NiFeCr layers enhance the magnetoresistance response and reduce the noise of the sensor. Another, recent work on the trilayer structure published by H. piskin and N. Akdogan based on the use of Pt interfacial layer between the NiFe and IrMn layers proves that the sensitivity increases by using the Pt layer. However, the hysteresis of the sensor is large [41]. Based on this optimization and result, the trilayer Planar Hall sensor promises to be an important device for the ultra-high sensitivity and ultra-high accurate applications such as the detection of the biological molecules, the characterization of magnetic materials, and the automotive applications.

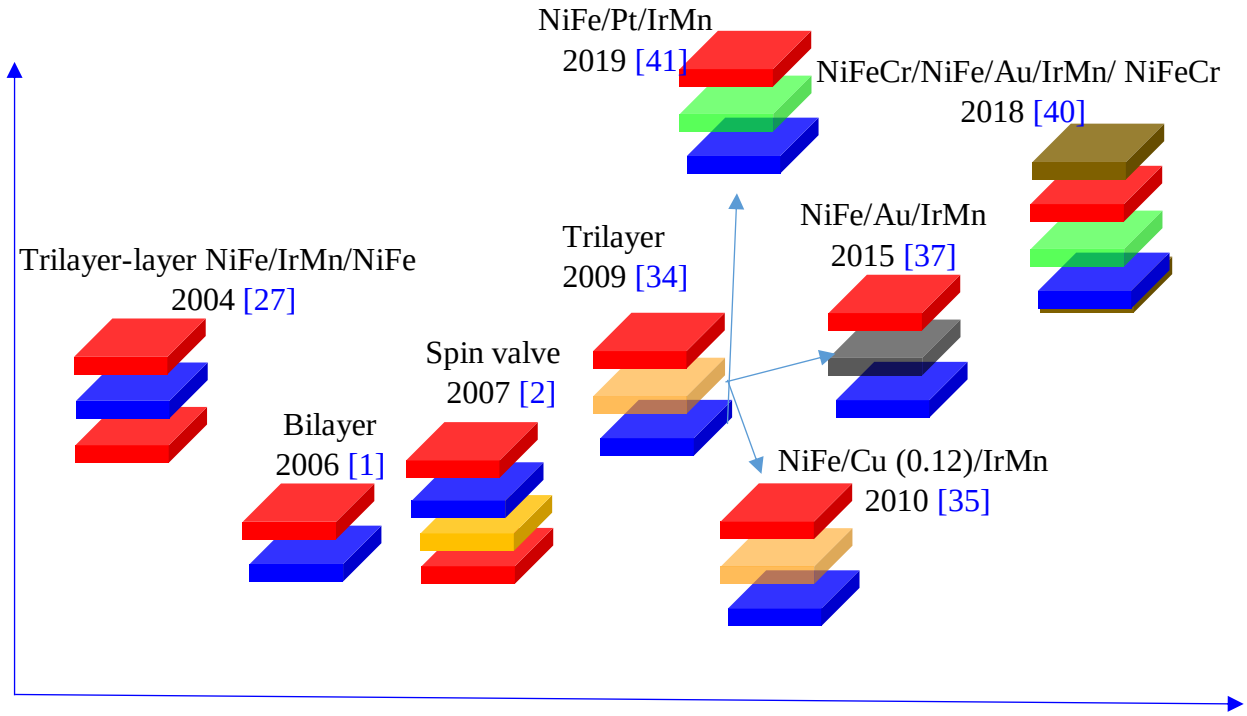


Figure 1.10 The most important structure development of the Planar Hall magnetoresistance sensor in the last thirteen years.

## 1.4 Shape development of the Planar Hall sensor

The change in the micro-shape of the magnetic materials could modify its magnetic proprieties or even induce the creation of new proprieties such as the anisotropic magnetoresistance, the multi-domain behavior …etc. Here we will present the different changes that have occurred in the form of the Planar Hall magnetoresistance sensor to change its sensitivity and enhance its properties. This section presents an important introduction to the chapter 3 in which we will discuss a theoretical study on the effect of the sensor's shape on the interaction between magnetic particles and the sensor, and we will also propose new forms of sensors that can enhance the detection of the nanoparticles that are difficult to detect using traditional sensor shapes.

### 1.4.1 Cross sensor

Over the last two decades, most studies on the Planar Hall sensor have been done on a cross-shaped sensor. The selection of this form was based on their easy manufacture not to mention the many studies that dealt with different physical phenomena emerging in these forms. Returning to the initial work of Schul and his colleagues [25], the study used a square junction Planar Hall sensor with an active surface of 28 µm × 28 µm. The authors mentioned in this paper that the change in the sensor's size does not have any effect on its performance. In the years following this discovery, most studies focused on changing the structure of the sensor with no attention to its shape. Ten years after this achievement, few studies focused on the effect of the sensor's size on its sensitivity. In 2007, the group of Pr. Kim studied the effect of the size of the cross junction on the sensitivity of Planar Hall spin valve sensor [42]. By studying three different sizes of the sensor, 50×50 $\mu m^2$, 20×20 $\mu m^2$ and 5×5 $\mu m^2$, they proved that the sensitivity increases with the decrease of the sensor's size. However the Planar Hall voltage decreases with the increase of the sensor's size. Another study concerning the effect of the size of the sensor was published by M. Donolato and his colleagues [43]. The study combines both experimental characterization of the Planar Hall sensor and micromagnetic simulation to understand the effect of different sizes of the sensor on its magnetic behavior. The work proves that the decrease in the size of the sensor induces the creation of tow easy axis on the surface of the sensor. Also, by studying different sizes of sensor's arms from 3 µm to 40 µm, M. Donolato and his colleagues demonstrate the increase in the sensitivity when the size of the sensor decreases. In addition, the theoretical work published by Hansen Group proves the decrease in the sensor's size induces the increase of the magnetic signal created by the magnetic bead [44]. These previous studies suggest that the sensor's size should be decreased in order to increase its ability to detect small magnetic fields. However, the following works which focused

on changing the shape of the sensor proved the possibility of increasing the sensitivity significantly without the need to reduce the dimensions of the sensor.

### 1.4.2 Tilted Cross-sensor

To enhance the sensitivity and the linearity of the Planar Hall sensor, another form of the magnetoresistance sensors was proposed by Hung and his collaborators based on tilted cross-sensor [4]. By combining both Planar Hall effect and anisotropic magnetoresistance, the sensitivity of this hybrid sensor is increased by about 30% for cross-junction tilted at an angle of 45°.

### 1.4.3 Bridge sensor

The Planar Hall sensor was usually manufactured based on cross-shaped Hall geometry. However, the famous paper of A. D. Henriksen highlighted the possibility to observe the Planar Hall effect in Wheatstone bridge topology [5]. The Planar Hall sensor output of the bridge geometry is a hundred times bigger than the conventional cross-shaped sensors. Furthermore, the authors found that the sensitivity of the sensor could be increased by increasing the number of the sensor's arms. Based on this achievement, the development of an ultra-high sensitive planar Hall sensor is introduced by changing its shape.

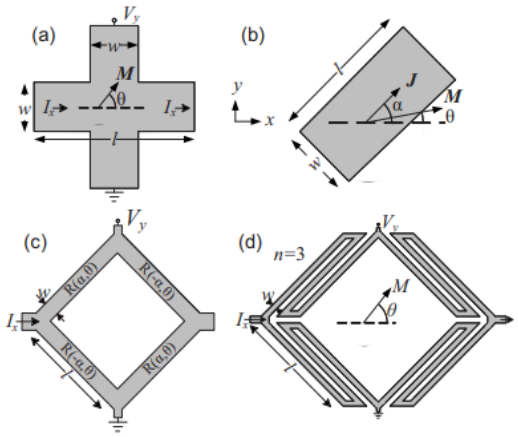


Figure 1.11 The cross junction Planar Hall magnetoresistance sensor. (b) The arm of the bridge Planar Hall magnetoresistance sensor. (c) The bridge Planar Hall magnetoresistance sensor with a single arm. (d) The bridge Planar Hall magnetoresistance sensor with three arms [5].

In the order to compare the performance of the new bridge sensor's geometry to the conventional cross's geometry, the research group of Pr. Hansen used both bridge and cross sensors to measure the Brownian relaxation of magnetic nano-beads [45]. They found that the bridge sensor yields six times bigger signals compared to the cross sensor. The high signal of

the bridge sensor makes it a promising device in the lab-on-a-chip applications. One year later, the same group optimized the geometry of the bridge sensor for magnetic bead detection [46]. Three different bridge sensors are studied to obtain the influence of both the external magnetic and the self-magnetic fields created by the sensor. The geometries include the conventional bridge geometry and two new ones. The first is called the pPHEB sensor and the second called the dPHEB sensor. Both latter sensors are insensitive to the external magnetic field and can only detect the bead's magnetic field created by the sensor's self-magnetic field.

### 1.4.4 Ring sensor:

The ring Planar Hall sensor which is based on the spin valve structure NiFe/Cu/NiFe/IrMn was fabricated by Sunjong Oh, et al in 2011[47]. The voltage profile combines the sum of both anisotropic magnetoresistance and Planar Hall effects. They found that the field sensitivity of the single ring sensor is 9.5 mΩ/Oe, and it increased up to 102.6 mΩ/Oe for 17 rings. B. Sinha and his teammates analyzed the role of PHR and AMR contribution in the multi-ring sensor of 7 rings based on ultra-sensitive trilayer structure [48]. They found that the sensitivity of the sensor increases linearly with the radius/width ratio of the sensor. In order to understand the magnetic behavior of the spin crossover materials at the nano scale, Hung and his colleagues used the ring planar Hall sensor to characterize ultra-low quantities of the spin crossover materials at room temperature [9]. Using this sensor they can detected ultra-low volume of spin crossover materials ($3\times10^{-3}$ $mm^3$). This ultra-low quantities could not be detected before at room temperature due to the limited detection of SQUID magnetometer and the high thermal noise of nano-SQUID magnetometer. The achievement opened the way to the use of Planar Hall sensor in new applications of ultra-low detection. Likewise, the ring planar Hall sensor contributed with the self-field detection method to characterize an ultra-low magnetic moment of $10^{-14}$ emu [10]. All these optimization make the ring sensor one of the important choices in magnetic field sensing applications.

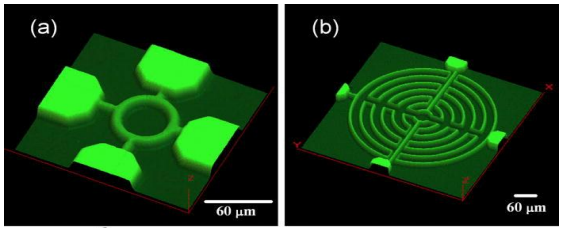


Figure 1.12 The ring Planar Hall magnetoresistance sensor (a) one planar Hall ring, (b) mluti-ring planar Hall [48]

### 1.4.5 Elliptical sensor

The elliptical Planar Hall sensor was developed by Pr. Klein's group based on the monolayer of Permalloy [49]. Using this geometry, the anisotropic magnetoresistance of the sensor could be induced without the need of the antiferromagnetic layer. To study the effect of the elliptical shape and size of the sensor on the magnetic response, the variation of the magnetic orientation, the linearity and the reversibility of the electrical response, the authors combined experimental, simulative and analytical studies of the elliptical planar Hall sensor. Two magnetoresistance sensors with minor and major axis of 0.65 µm/2.44 µm and 0.83 µm/ 3.29 µm were created. They found in this study that the ratio between the two axes and the thickness of the sensor strongly affected the response of the sensor. A high response of the sensor could be induced by increasing the ratio between the elliptical size and the thickness of the sensor. However, the increase of the minor axis could induce a hysteresis and the decrease of the sensor's thickness could reduce the Planar Hall signal.

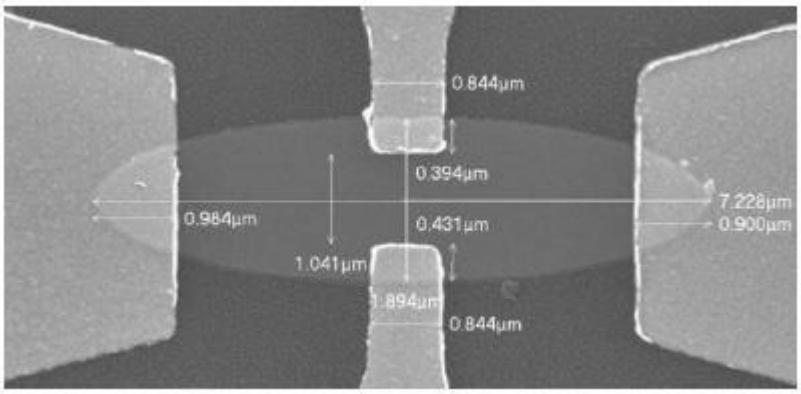


Figure 1.13 A high resolution scanning electron microscope image of a Planar Hall magnetoresistance elliptical sensor [49]

Two years after this study, the same group proved the existence of mono-domain behavior in elliptical shape of Permalloy thin films with a long axis ranging from several microns to several millimeters. The study proves the existence of monodomain behavior in the sensor even when its size is large. These results advantage the sensor because a large elliptical sensor have a small anisotropic field which induces the high sensitivity of the sensor [50]. After these achievements, Pr. Klein's group focused on improving the resolution of the Planar Hall elliptical sensor to the order of 1 nT/√Hz [51] and 600 pT/√Hz [52] at ultra-low frequency (0.1 Hz). So far, this sensor has not been used in biological applications, but the high resolution of this sensor suggests that it will be one of the sensors required in various technological and biological applications.

## 1.5 Other optimizations of the planar Hall sensor

In addition to the works which dealt with changing the shape of the sensor or its structure, other works dealt with the possibility of improving sensor sensitivity through the development of new ideas for sensing. In this section, we present some scientific works which dealt with the development of the sensing method such as the use of the self-field method or changing the angle between the external magnetic field and the easy axis of the magnetoresistance sensor.

The self-field detection is a new method of the biological detection by the Planar Hall sensor based on the use of the intrinsic magnetic field created from the sensor to magnetize the magnetic bead. The theoretical work published by the group of Pr. Hansen under the title "Theoretical Study of In-plane Response of Magnetic Field Sensor to Magnetic Beads Magnetized by the Sensor Self-field" [53] studied the interaction between the Planar Hall sensor and the magnetic beads that are magnetized by the self-magnetic field of the sensor. The study proves the advantages of this approach compared to the conventional method, where the magnetic field created by magnetic beads has the same direction (sign) whatever the position of the magnetic bead is. However, when we apply an external magnetic field, the magnetic field created by beads outside the sensor has the inverse (direction) sign to the magnetic field created from the beads inside the sensor. Therefore, the global magnetic field created on the sensor will reduce. Based on this advantage, the self-field methods are largely used in the biological detection to magnetize the magnetic beads [54-56]. On the other hand, the magnetic field created from the bead is proportional to the square of the bias current. This means that the increase of the bias current induces the increase of the magnetic field created from the bead. However, the high current induces the joule effect which could break the sensor or affect its accuracy or even change the state of magnetic particles or biological molecules during the measurement. To understand the maximum bias current that can be used without breaking the sensor, the group of Pr. Hansen presented a systematic study of the self-heating of planar Hall magnetoresistance sensor based on bridge geometry [57]. The experiment results in this study were supported by the finite element simulation and analytical thermal model. The study proves that the use of the large width of the sensor induces a small change in the temperature under the effect of the current. The same group optimized the sensor stack of the Planar Hall sensor for biological detection using self-field method [58]. Another application of the Planar Hall sensor appeared when Hung and his team characterized ultra-low quantities of spin-crossover materials at room temperature [10] by combining both the high sensitivity of the ring geometry of the sensor and the self-field method. This study opened the door to the possibility of using

the magnetic sensor as a very effective tool in the magnetic characterization of magnetic nanoparticles. Also to compare the trilayer structure and the bilayer structure, a trilayer structure based NiFe/Cu/IrMn with different sizes of the ferromagnetic and the nonmagnetic layers was studied by measuring the sensor's response as a function of the external magnetic field and also under the effect of the magnetic field created from the magnetic bead. The authors found that the signal of the trilayer structure based on NiFe (20 nm or 30 nm)/ Cu (0.6 nm)/ IrMn (10 nm) is higher than the bilayer structure which is usually used for the self-field applications [59]. Parallel to the works that use the self-field to increase the sensitivity of the sensor and improve the bead sensor interaction, another work is done by the Pr. Ferial's group and Pr. Kim's group discussed the possibility of improving the sensitivity of the sensor by changing the angle between the external magnetic field and the electric current. They found that the sensitivity of the sensor increases 3.6 times when the angle between the external magnetic field and the current direction equals 20°. By using this optimization, the authors proved the possibility of detecting an ultra-low magnetic moment of $4\times10^{-13}$ emu [60]. The group of Pr. Kim proposes the application of the external magnetic field in the z direction of the sensor. This method allows the application of a high external magnetic field without saturating the magnetic sensor (because the magnetization of the sensor is very strong in the direction of the easy axis of the sensor) [61]. The magnetic moment resolution achieved by this method is in the order of $10^{-10}$ emu.

## 1.6 Conclusion

In this first chapter, we present the theoretical background of the Planer Hall effect, illustrating the various physical phenomena that give rise to this effect. This chapter also provides a solid ground for an understanding of the various developments that have been made on the planar Hall sensor, both those related to changing of the structure (bilayer, spin valve, and trilayer) of the sensor or those aimed to improving the properties of the sensor by changing its shape (bridge, ring, and elliptical sensor). Concerning sensor-shape studies, these studies represent an important introduction to the chapter 3, in which we discuss the results of numerical calculations that aim to improve sensor response by changing its shape. Also we mentioned in this chapter several works that have contributed to improving the sensor response by relying on new detection techniques such as the self-field technique. We have also presented some of the most important researches on the use of these new techniques, whether to characterize magnetic nanoparticles or to detect biological molecules.

# 2. Experimental techniques

## 2.1 Introduction:

In this chapter, we will introduce the techniques used in the sensor manufacturing process and that used to characterize its electromagnetic behavior. We will introduce the magnetron sputtering system, the photolithography technique, the SQUID magnetometer, and magnetomesurement techniques.

## 2.2 The manufacture of the sensor

In this section, we will present briefly the technical method for manufacturing the Planar Hall magnetoresistance sensor. The sensor's manufacture is divided into two basic stages: the first stage is the sputtering of the magnetic layers, and the second stage is the inscription of the sensor. In the first stage, a magnetron sputtering system is used to create the sensor stack and in the second stage, a lithography technique is used to print the Planar Hall magnetoresistance sensor.

### 2.2.1 Magnetron sputtering system:

Except for some works which used MBE (molecular beam epitaxy) method to produce the Planar Hall magnetoresistance sensor (such as the first work on the planar Hall sensor published by Shul [25]), most Planar Hall magnetoresistance sensors were usually manufactured based on a magnetron sputtering system. The magnetron sputtering system is largely used for the deposition of metal and also for the deposition of some dielectric materials. The first sputtering system was developed by Peter J. Clarke [62] which led to a quantum leap in the semiconductor industry. There are two global magnetron sputtering systems. First, DC magnetron sputtering system which is used for metals and, second, RF magnetron sputtering system which is used for dielectric materials. The DC magnetron sputtering system consists of a cathode (the target or the source) and an anode (the wafer or the substrate) in a vacuum room containing an inert gas which is usually Argon due to its low reactivity. The principle of operation of this device in its simple form is based on the application of a difference of voltage between the anode and the cathode. This difference of voltage leads to the creation of plasma in the vacuum room; consequently, the electrons travel from the cathode and collide with the atoms of Ar which induce the ionization of Ar atoms positively. The ions of Ar+ attract to target with a high velocity which induces the sputters of the target atoms due to the momentum of collisions. Then, the atoms of the target are deposited on the substrate in the form of a thin film of material. In order to increase the density of the plasma close to the target, a magnetic field should be applied parallel to the target. This induces the spiral movement of the electrons

around the magnetic field. The ionization of the sputtering gas enhances and the deposition rate increases. The quality of the magnetic layers depends on the different parameters of the sputtering system such as the vacuum of the room, the density of Ar gas, the amplitude of the DC voltage…etc. For our thin films magnetoresistance sensor, we use the following conditions:

The base pressure in the main chamber was $2\times10^{-5}$ Pa. Working pressure of the system during the deposition is 0.4 Pa controlled by the automatic shuttle gate with Ar gas flow rate of $5 \times 10^{-7}$ $m^3/s$. To acquire homogenous layers, the substrate holder was rotated at 10 round per minute during the sputtering. In order to induce the easy axis of the sensor, a uniform DC magnetic field of about 20 mT was applied in the plane of the thin film. Also, the deposition rates of NiFe, Cu, IrMn, and Ta layers are 0.064 nm/s, 0.038 nm/s, 0.108 nm/s and 0.06 nm/s, respectively with an error of 5% for all layers.

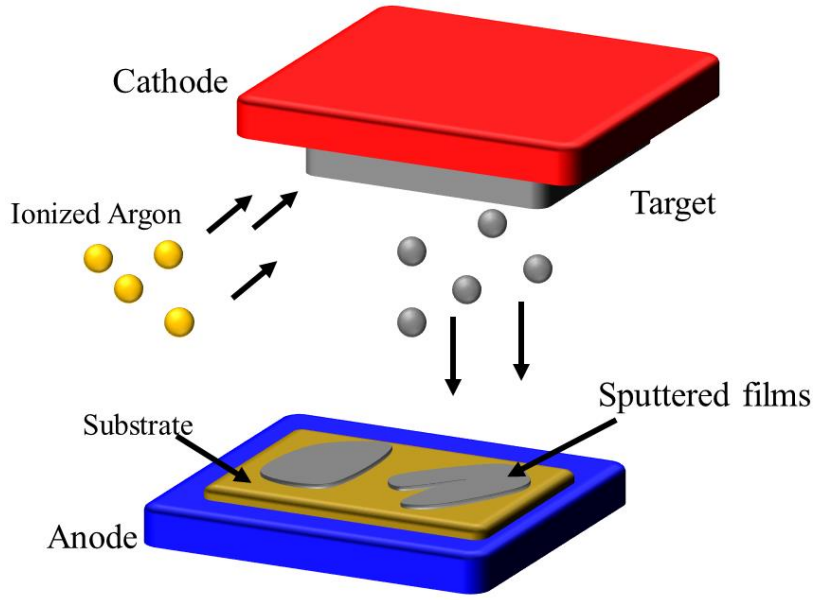


Figure 2.1 the DC spurting magnetic system.

On the other hand, in the case of Radio Frequency (RF) magnetron sputtering, the DC source power is replaced by an AC source power. This system is commonly used for the deposition of insulating materials such as aluminum oxide, silicon oxide, and tantalum.

### 2.2.2 Photolithography:

The thin magnetic layers manufactured by the magneto sputtering system cannot be used as a magnetic sensor. In order to manufacture the magnetoresistance sensor and the electrical contact, the photolithography technic is used. The idea of optical printing is based on the transfer of geometric shapes on a mask to a smooth surface. The name Photolithography is divided into three words: Photo meaning light, litho meaning stone, and graphy meaning write.

This technique is introduced for the first time by Alphonse Poitevin in 1855 [63]. In general, this technique is divided into different steps that are summarized as follows:

1/ Wafer (substrate) cleaning: The first step in the photolithography technique is removing the different particles located on the wafer such as metallic, organic or inorganic impurities by chemical cleaning. This step is a very significant step because any existence of small quantities of impurities could reduce the quality of the magnetic sensor.

2/ Barrier formation: The next step is the growth of the oxidation layer to the surface of the wafer, normally, due to its high surface energy (2130 ergs /$cm^2$) [64] the silicon surface will be oxidized automatically when it is exposed to air. However, the normal oxidizing layer which forms by the contact of the wafer with the atmosphere has a very thin thickness (between 1.5 to 2 nm). This silica layer cannot be used as a barrier layer, and this requires the growth of the SiO layer on the wafer.

3/ Photo resist: The third step is the growth of the photo resist layer on the silica layer. To grow the layer of photo resist, we use the spin coating process where the solution of polymer spread evenly on the surface of the silica using the centripetal force. This method allows the creation of relatively uniform thin photo resist films. The quality of these films depends on several parameters such as the spin speed (RPLM) and the duration of spinning. There are two major types of the photo resist, the positive photo resist and the negative photo resist. For the first type, the application of a UV light induces the degradation of its proprieties and it becomes more soluble than the unexposed photo resist. Then the exposed photo resist could be washed away by a developer solution. For the second type, the application of UV light induces the enhancement of its proprieties and thus becomes less soluble than the unexposed photo resist, so the photo resist which is not exposed to the light could be washed away by a developer solution. The figure below summarizes the difference between the negative and the positive photo resist.

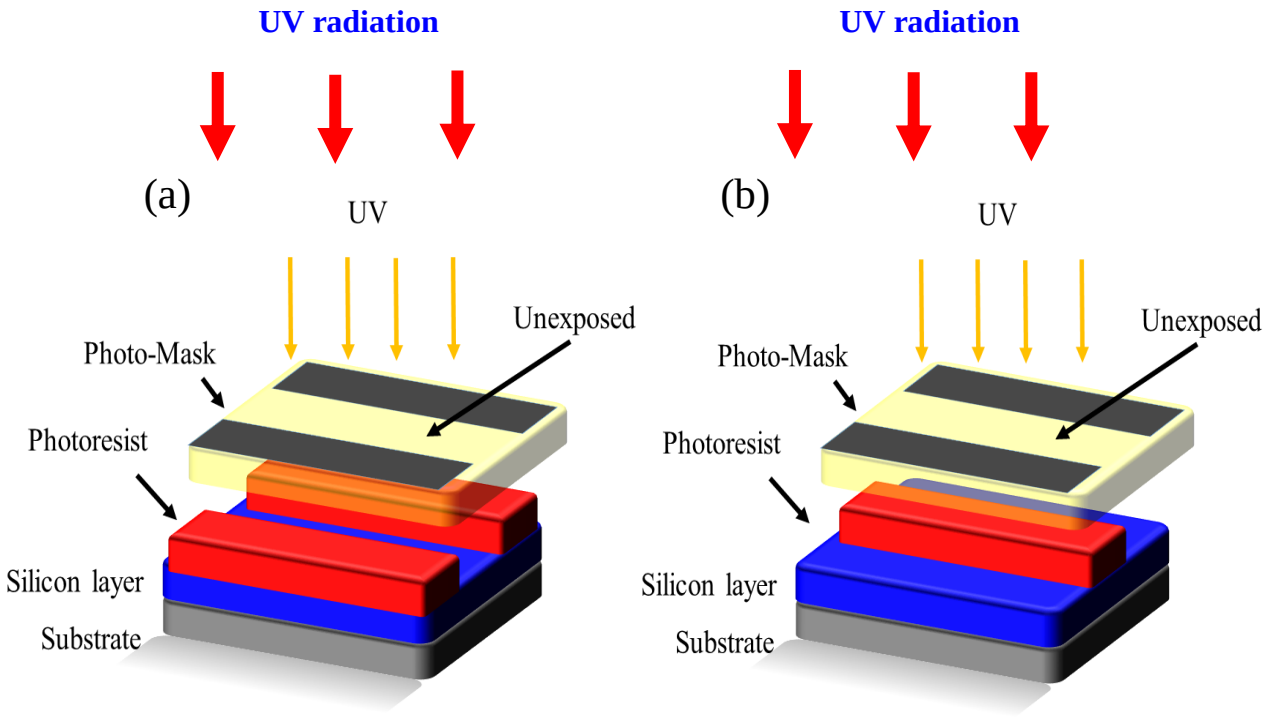


Negative photo resist positive photo resist

Figure 2.2 (a) The Negative, and (b) the positive photo resists.

Mask: After the deposition of the photo resist, the photomask should be used to make the shape of the sensor (or the electrical circuits). The photomask is an opaque plate with transparent zones that allow the UV radiation to pass through. The zones where the photomask does not cover the photo resist will be affected by the UV radiation, and because the photo resist is a special class of the photosensitive polymer, the light will change the proprieties of the photo resist. Consequently the proprieties of the photo resist in the zone covered by the mask and the zone not covered by the mask are not the same.

Development: after the radiation of the photo resist by UV light, a chemical treatment should be used to etch the unexposed zone of the photo resist (case of the positive photo resist). After this step, the magnetic layers, the electrode or the passivation layer could be deposited (by sputtering) on the wafer. This step will follow the cleaning process to resist the phot, and only the part that is not covered by the photo resist is retained. Thus, the sensor is manufactured in the desired form. The different steps of the photolithography are summarized in the figure below:

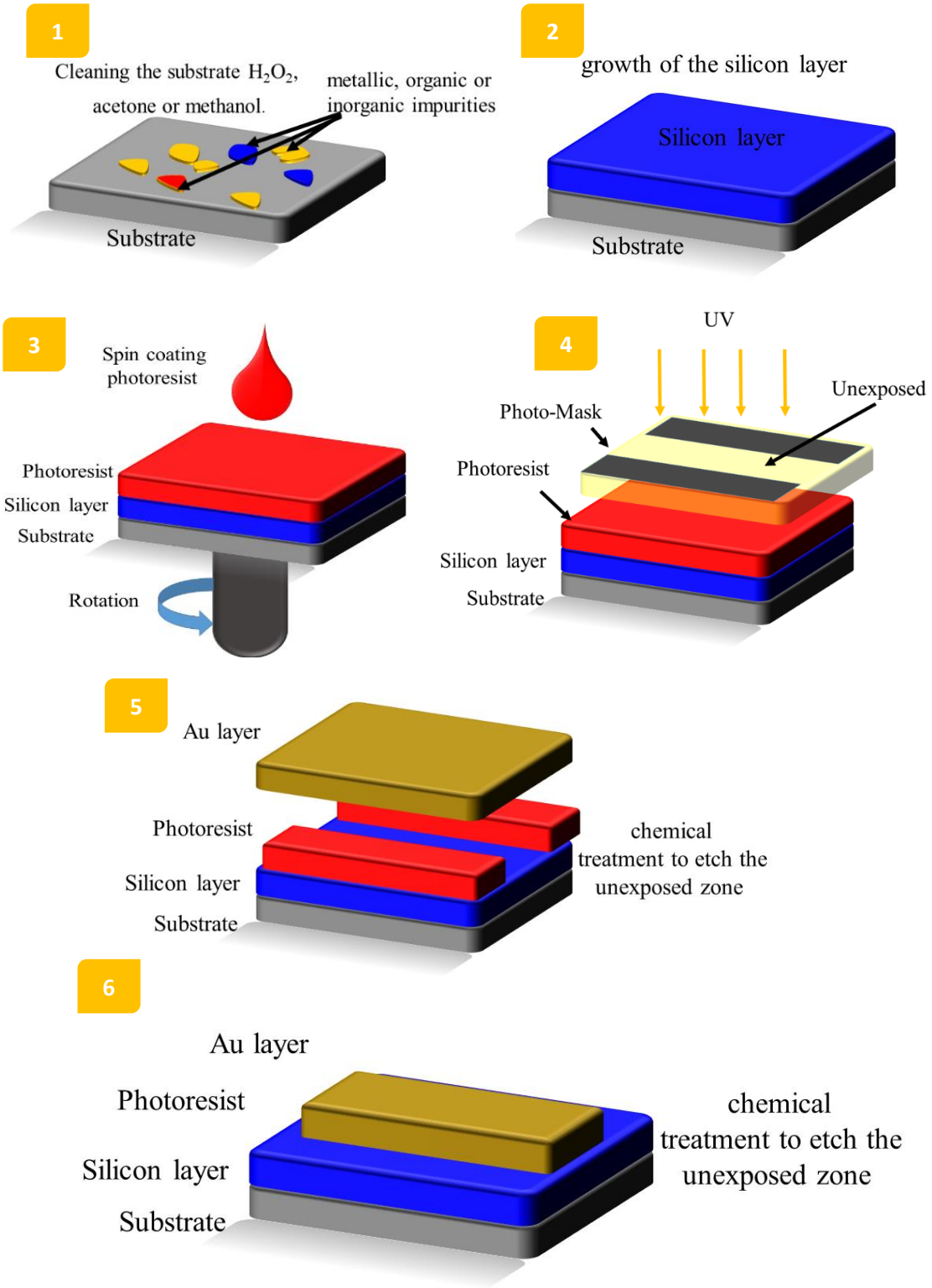


Figure 2.3 The different steps of the photolithography technique for the manufacture of the electrodes 'the same steps will be used for manufacturing the other components of the sensor such as the sensor junction or the passivation layer).

## 2.3 Characterization techniques:

In this section we present some technique used to characterize the behavior of the planar Hall magnetoresistance sensor.

### 2.3.1 The magnetoresistance measurement:

The magnetoresistance measurement technique is a common unexpansive technique used to characterize the properties of the thin films of magnetic materials. The advantage of this characterization method is its ability to detect some behaviors that cannot be detected using traditional techniques such as its ability to detect the dynamics of the magnetic moments in the antiferromagnetic materials [65] or its ability to detect a small change of the easy axis of magnetization of the ferromagnetic thin films under the effect of the temperatures (see chapter V). To characterize the planar Hall sensor a current usually applied in the easy axis of the sensor and a magnetic field applied in the hard axis of the sensor. The applied magnetic field induce the change of the magnetization of the sensor from the easy axis to the hard axis which induce the change of the electrical response of the sensor. This caharcterization gives information about the anisotropic resistivity of the sensor. To characterize the change of the easy axis, the exchange bias field, and the coercivity field as a function of the temperature the external magnetic field should be applied in the easy axis of the sensor. The change of the easy axis direction appease in the change of the shape of the electrical response of the sensor from symmetrical response to unsymmetrical response, the change of the exchange bias field reflected by the change of the shift of the planar Hall voltage loop, and the change of the coercivity filed appease by the change of the width the planar Hall voltage loop.

### 2.3.2 Superconducting Quantum Interference Device (SQUID) Magnetometers:

The Superconducting Quantum Interference Device (SQUID) is one of the most used devices for characterizing magnetic properties of materials. The operation of this device based on two main phenomena, one is the superconductivity, and the second is the Josephson junction. Superconductivity is a phenomenon observed more than a century ago by the physicist Heike Kamerlingh Onnes. He observed that the electrical resistance of mercury disappears when it is cooled at -269 °C. Another phenomenon associated with the superconductivity called the Meissner effect were external magnetic fields which applied to the superconductivity material will not penetrate the superconductor, but remain at its surface. On the other hand, the Josephson effect is a phenomenon of supercurrent, a stream that flows indefinitely long without any applied voltage, via a device known as the Josephson Junction, which consists of two or more superconductors coupled with a weak conductor. The Josephson effect was named after the British physicist Brian Josephson, who in 1962 predicted the phenomenon. The SQUID

consists of a superconducting loop interrupted by two Josephson junction were a current passes through them. When the magnetic flux change, the maximum super current will oscillate as a function of the magnetic flux. In our work we use the SQUID to characterize the magnetic proprieties of planar Hall cross sensor via its magnetization loop at room temperature as we will present in chapter 4.

# 3. The Thermal Behavior of the Planar Hall Magnetoresistance Sensor

## 3.1 Introduction

A wide range of applications of the magnetoresistance sensor requires the use of the sensor in an unstable thermal environment. These applications include the bio-medical applications where the magnetoresistance sensor is used to detect the effect of temperature on some biological molecules such as DNA [7], protein [68], the position sensing which includes some industrial applications and automotive applications [69], the characterization of the Nano-magnetic particles [9, 10], the navigation and transportation systems [70] and the space applications [12]. However, the change in temperature induces the change in the magnetic and the electric states of the magnetoresistivee sensors which affect the sensitivity and the thermal stability of the sensors and lead to inaccurate measurements. To overcome this problem, compensation systems were proposed to correct the error of the measurement. These compensation systems could be an electronic device [69] or a mathematic algorithm. In the case of the Planar Hall magnetoresistance sensor, the group of Pr. Hansen used a reference sensor to correct the error of the measurement for the biological applications. This study focused on the behavior of the sensor from -10 °C (263 K) to 70 °C (343 K) [71]. However, the use of a second sensor complicates the sensing processes and increases the cost of the sensing operation. This leads to limiting the use of the sensor for other applications such as the space application where the size of the electronic device is a critical parameter. Other works propose the change of the Cu space layer in the trilayer structure of the sensor and the use of Au layer to increase the thermal stability of the sensitivity of the magnetoresistance sensor [37]. However, the dependence of the sensitivity on the temperature in this case is steel high (the temperature coefficient of the sensitivity of the trilayer NiFe/Au/IrMn is 0.25 %/K) and the range temperature of this study change from -20 °C to 60 °C. This range does not include the space application or the characterization of some magnetic materials which have different properties as a function of the temperature or even some automotive and industrial applications.

In this chapter, we will study the behavior of planar Hall sensors as a function of the temperature. The chapter will be divided into three sections, in the first section, we will present a new method to increase the thermal stability of the magnetoresistance sensor's sensitivity in a wide range of temperature from 110 K to 360 K (corresponding to -163 °C to 87 °C) without the need to add other electronic devices or change the magnetic stack of the sensor. This method

reduces the temperature coefficient of the sensor to 0.02%/K which is more than 12 times smaller than a recent achievement in the Planar Hall sensors [37] and could reduce the limit of the detection of the sensor to $10^{-15}$ emu. This high thermal stability is comparable to the stability of the Tunnel magnetoresistance sensor sensitivity [72] and higher than the stability of the giant magnetoresistance sensor sensitivity [73] and that of the anisotropic magnetoresistance sensor sensitivity [74]. Note that for these previous studies, the range of the temperature is smaller than our study. High thermal stability of sensitivity in a wide range of temperatures could open the way to the use of the Planar Hall sensor in new areas of applications such as the automotive and the space application, and reduce the complexity and the cost of biosensor devices. On the other hand, the replacement of conventional devices (SQUID) currently used in the academic field to study the magnetic properties of some materials is a major objective not only because of the high sensitivity of the magnetic sensor but also for its low cost compared to conventional devices (SQUID 1 million $, and Planar Hall magnetoresistance system 30 $). In addition to this high thermal stability of sensitivity, we will present in this section the global picture of the behavior of the Planar Hall magnetoresistance sensor as a function of temperature. The change in the different magnetic parameters of the sensor such as the exchange bias field, the anisotropic field and the difference between the resistivity parallel and perpendicular to the magnetization will be studied as a function of temperatures. Also, we will prove the existence of a small change in the angle of the easy axis when the temperature increases. In fact, this change observed before in the bilayer (FM/AFM) structure and due to the limit of the sensitivity of the measurement device was attributed to a fault in the external magnetic field orientation [75].

In the second section of this chapter, we will study the behavior of the planar Hall bridge sensor for a harsh thermal environment by studying the variation of the signal voltage, the offset, the sensitivity, the durability, and the detectability of the sensor in the range of temperature from -80 °C (193 K) to 140 °C (413 K). This study aims to investigate the behavior of the sensor for space and industrial applications and its ability to withstand the harsh thermal environment for long periods. We will also highlight the high thermal stability of the sensor in this harsh thermal environment, which exceeds the thermal stability of other magnetoresistance sensors (temperature coefficient of the sensor to 0.003%/K). This high stability of the sensitivity was achieved by applying an electrical voltage to the sensor rather than applying an electric current. Moreover, we show that the application of a high magnetic field at high temperatures induces a transition of the anisotropic magnetoresistance from uniaxial magnetic anisotropy to biaxial magnetic anisotropy. The other parameters of the sensor such as the exchange bias field

and the coercivity field as well as the anisotropic resistivity was investigated as a function of the temperature. Also, we study the variation of the offset voltage, the thermal noises, and the durability of the sensor.

In the section three, we will study the behavior of planar Hall ring sensor for ultra-low temperature. The variation of signal voltage, the offset, the sensitivity, and the detectability in the range of temperature between -268 °C (5K) to 37 °C (310 K) will investigated. This study aims to understand the behavior of magnetic sensor at a low temperature in order to apply it in the detection of nanoparticles such as the gold nanoparticles at low temperature or the space applications. We note here that the planar Hall ring sensor was used to characterize the gold nanoparticles at room temperature and the results of these characterizations will present in the chapter five. However, the behaviour of these nanoparticles as a function of the temperature it could be the target of future applications.

## 3.2 High thermal stability of magnetoresistance sensor sensitivity

### 3.2.1 The sensor structure:

Below the Néel ($T_N$) temperature (generally $Tc > T_N$), the magnetoresistance anisotropy of a ferromagnetic layer (FM) such as NiFe can be strengthened by contacting the FM layer with an antiferromagnetic layer (AFM) such as IrMn. This phenomenon is the product of the interaction between the magnetic moments in the two layers (FM and AFM), which is known by the term “exchange bias interaction”. This phenomenon was discovered 63 years ago by Meiklejohn and Bean [76]. The exchange bias appears clearly in a shift of the hysteresis cycle of the magnetization $M$ ($H$) from the zero when the FM layer is not coupled to AFM layer to non-zero values for the FM/AFM coupled structure. The values of the magnetic field shift known as the exchange bias field.

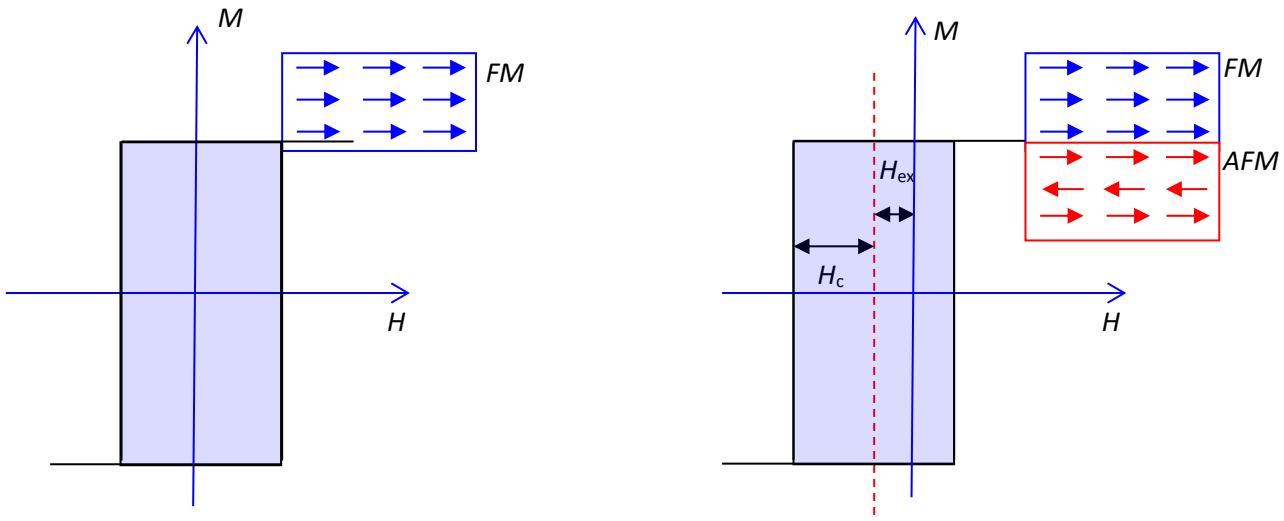

Figure 3.1 The hysteresis loop for (a) a ferromagnetic layer and (b) a ferromagnetic / antiferromagnetic bilayer. The shift of the hysteresis cycle *M* (*H*) is induced by the effect of the exchange interaction between the two magnetic layers.

This exchange bias field induces the "unidirectional" anisotropy. This means that when an external magnetic field is applied perpendicularly to the easy axis, the magnetization change from 0 to 90 degrees as the magnetic field increases, and it goes back to a decrease from 90 to 0 degrees when the external field decreases. These are very important characteristics where the Planar Hall signal show a reversal behavior. However, due to the exchange bias field, the magnetic moments in the FM layer becomes more resistant to the external magnetic fields. The rotation of the magnetic domain in the case of an FM / AFM bilayer requires a stronger external magnetic field than that applied for the rotation of a single ferromagnetic layer. As a result, the magnetic FM layer becomes less sensitive to the external magnetic field. The low sensitivity of the FM layer is a negative point in the use of this type of structure (FM / AFM) as a magnetic field sensor (the FM layer used as a sensitive layer of the sensor). However, N. J. Gökemeijer [77] and his colleagues show the possibility of weakening the exchange field by the isolation of the FM and AFM layer using a non-magnetic spacer layer (FIG.4.2.a). The interaction between the FM and AFM layer, in this case, becomes an indirect interaction that is weak compared to the direct interaction. Also, the increase of the thickness of the spacer layer induces an exponential decrease in the value of the exchange field (FIG.4.2 b). The weak exchange interaction between the two magnetic layers (FM and AFM) releases the magnetic moments of the FM layer and therefore the tri-layer must be more sensitive to external magnetic fields compared to the bilayer.

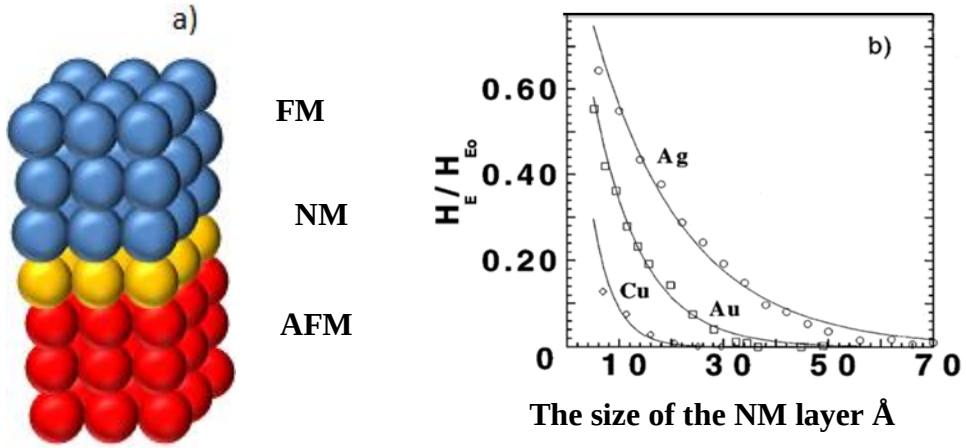


Figure 3.2 Trilayer structure based on (FM/NM/AFM) layers. b) The variation of the exchange biased as a function of the thickness of the non-magnetic layer.

The optimization of the sensitivity of magnetic sensors by the use of a tri-layer structure is reported the first time by Hung and his colleagues in 2009 [34] and the values of the thickness of the non-magnetic layer were optimized by the same group in 2010 [35]. They show that the magnetic tri-layer based on NiFe (10 nm) / Cu (0.12 nm) / IrMn (10 nm) structure has high sensitivity compared to the bilayer or spin valve structures. The paper of Xu-jing Li showed the possibility of increasing the sensitivity of the sensor by increasing the thickness of the non-magnetic layer up to 1 nm [78]. The exchange field in this case must be zero. Other studies used the Au layer to increase both sensitivity and the thermal stability of the sensor [37]. Also, trilayer structure based on Pt non-magnetic layer shows a high sensitivity. However, this structure also shows a high hysteresis [41].

In our study, we used a Planar Hall effect sensor composed by three layers: NiFe FM layer (10 nm), a non-magnetic layer of copper (0.12 nm) and an AFM layer of IrMn (10 nm). FIG.4. 3 (a) shows the SEM image of the cross junction of the Planar Hall sensor. The width of this sensor is 50 µm with a 5 nm Ta capping layer and seed layer all deposited on $Si/SiO_2$ (625/0.5 µm) and substrate using a DC sputtering system. FIG.4.3 (b) shows the variation of the magnetization $M$ ($H$) at room temperature. In the same figure, the trilayer structure is drawn to clarify the non-homogeneity of the Cu non-magnetic layer. The trilayer structure was imaged using a high-resolution transmission electron microscopy (HRTEM) system as shown in FIG. 3.3 (c) Ta layers have an amorphous structure while NiFe and IrMn are in polycrystalline structure. Lattice fringes characteristic of IrMn (e.g., (101)–0.22nm) and NiFe (e.g., (111)–0.19nm) can be clearly seen from the HRTEM image. In addition, the thicknesses of NiFe, IrMn and Ta are determined by averaging 10 measurements at different areas along with the cross-sectional view. Their respective values are 10 ± 0.5 nm, 10 ± 0.6 nm, and 5 ± 0.25 nm. Despite these precise quantifications, the nominal Cu atomic layer of 0.12 nm sandwiched between NiFe and IrMn layers could not be visible due to the resolution limit of HRTEM imaging and the close similarity between the atomic weight of Cu and NiFe.

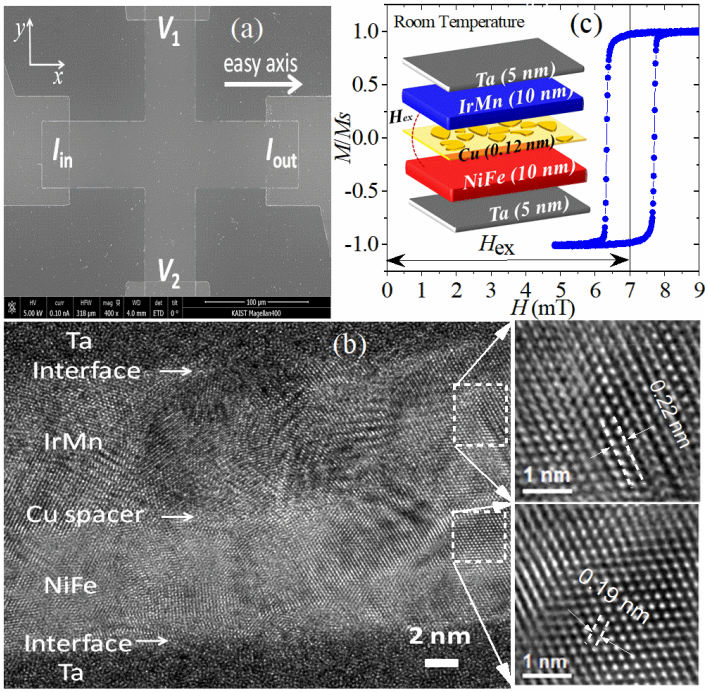


Figure 3.3 (a) A top view SEM image of a crossed junction of the sensor (the bar width is 50 lm; easy axis, electrodes for applied current and measured voltage of the junction are indicated). (b) Cross-sectional HRTEM image of the thin film stack Ta(5 nm)/NiFe(10 nm)/Cu(0.12 nm)/IrMn(10 nm)/Ta(5 nm). The TEM specimen was created using a focused ion beam (FIB, Hitachi NB 5000). The insets (1) and (2) show zoomed areas from NiFe and IrMn layers where the electron beam went through (101) and (111) zone axes of IrMn and NiFe nanocrystals, respectively. (c) Room temperature M-H hysteresis loop of the thin film; the saturation magnetization Ms 0.4 MA/m.

### 3.2.2 Stoner-Wohlfarth model:

One of the methods for simulating the magnetic behavior of materials is the micro magnetism model. The basic principle of micro magnetism model is that a magnet is a continuous medium in which the atomic-scale structure can be ignored. Although complete micro-magnetic models can better describe uniform and non-uniform magnetization processes, their numerical efficiency is much lower which explains why phenomenological models are still widely used in simulations. To find the physical parameters of our Planar Hall magnetoresistance sensor such as the exchange bias field, the anisotropy field, the easy axis angle and the anisotropic resistivity, we simulated the behavior of the sensor by the Stoner-Wohlfarth model. The Stoner-Wohlfarth is a classical model proposed by Edmund Clifton Stoner and Erich Peter Wohlfarth in a publication in 1948 under the name "A Magnetic Hysteresis Mechanism in Heterogeneous Alloys" [79]. This model is designed to describe the

behavior of magnetization in a ferromagnetic material. In this model, the magnetic particle is an ellipsoid uniformly magnetized with the existence of a uniaxial anisotropy. The uniform inversion of the magnetization of this particle under the effect of an external magnetic field is carried out by a coherent rotation, and the total energy of the particle in this case can be given by the following relation:

$$E = K_u\, t\, sin^2(\theta) - M_s t\, H \cos(\alpha - \theta) \qquad (4.1)$$

With:

*E*: the total energy of the magnetic particle.

*K*u: the constant of anisotropy.

*t*: the thickness of the FM layer.

$\theta$: the angle between the magnetization and the axis of easy magnetization.

*M*s: magnetization.

*H*: the external magnetic field.

$\alpha$: the angle between the applied magnetic field and the axis of easy magnetization.

The first term of energy, known as the anisotropy energy (the anisotropy energy can be induced by the shape of the magnetic films, the crystalline symmetry of the magnetic materials, the stress, and by the application of an external magnetic field on the ferromagnetic material during the growth of the magnetic layers). The magnetic field associated with this energy is called the anisotropy field and could be defined as the necessary field to saturate the magnetization along the axis of difficult magnetization:

$$H_c = \frac{2K_u}{M_s} \qquad (4.2)$$

The value of the anisotropy constant ($K_u$) varies between 0.1 and 104 kJ / m. The second term of energy is the Zeeman energy. The origin of this energy is the effect of the external magnetic field on the magnetic material. Then the total energy of the system is the result of the competition between the energy of Zeeman and the energy of anisotropy. The stable state of the system is corresponding to the minimum energy of the system. There are several methods to find the minimum of the system. One of these methods is to derive the equation of the energy and solve the equation d$E$ / d$\theta$ = 0 using a numerical method (because it is impossible to solve these kinds of equations using analytical method) such as Newton method. However, the disadvantage of the conventional numerical methods is the possibility of falling into a local solution of the equation, that is to say, the solution of the equation converges to a local minimum. The use of some modern mathematical methods such as the genetic algorithm which

is based on the natural selection principle [80] or simulated annealing [81], or the most modern technique which is called particles swarm [82] could be a good choice for this kind of problem.

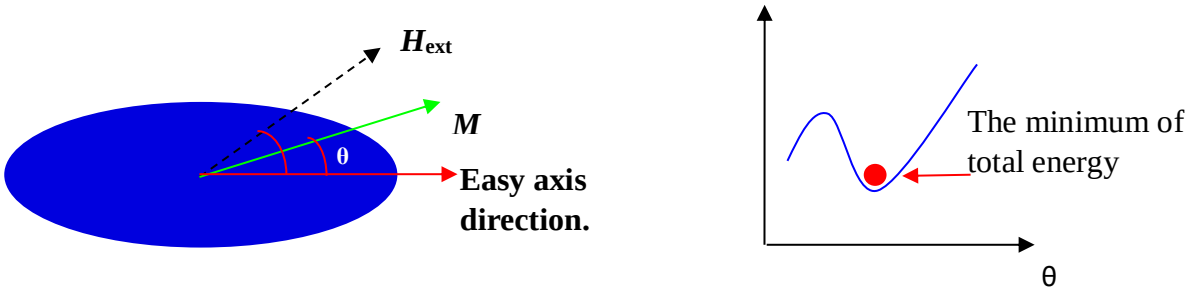


Figure 3.4 The ferromagnetic elliptical particle under the effect of the external magnetic field.

The figure 4. 4 shows the ferromagnetic elliptical particle with one easy axis under the effect of the external magnetic field. The variation of the magnetization of the magnetic domain could be simulated using the Stoner-Wohlfarth model where the expression of the magnetic particle is done as:

$$M = M_s \cos(\alpha - \theta) \qquad (4.3)$$

The angle $\theta$ obtained by the minimum of the equation of the energy.

By using the Stoner-Wohlfarth model we calculated the variation of the magnetization of a ferromagnetic layer as a function of the external magnetic field as shows the FIG. 4.5 The angle $\theta$ obtained from the minumu condition of the energy using the genetic algorithm method.

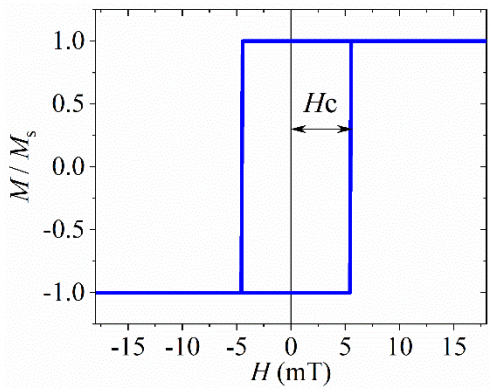


Figure 3.5 The magnetization curves of the Stoner-Wohlfarth model for angle α = 0°.

The figure 4.5 represents the magnetization curves (represented by the equation of the magnetization 4.3) as a function of the external magnetic field for $\alpha = 0°$. The hysteresis appears and the magnetization loop has a square shape. This hysteresis is due to the contribution of the domain walls in the reversal of the magnetization.

The assumption that all ferromagnetic materials consist of a single magnetic domain oriented along the axis of easy magnetization lead to conclude that all ferromagnetic materials act as a permanent magnet. Obviously, this does not happen in nature. In the case where the ferromagnetic has a micrometric size, the magnetic domain discharges several magnetic domains to minimize the total energy. The orientation of the magnetic domains is unordered, and the magnetic domains are separated by regions that are called the domain walls.

In the case of the bilayer FM/AFM, the exchange interaction between the two layers fixes the magnetic moments in the FM layer following the axis of easy magnetization. The magnetic domain in this case can be considered as a single magnetic domain, and the total energy of the FM layer can be given by:

$$E = K_u\, t\, sin^2(\theta) - M_s t\, H \cos(\alpha - \theta) - M_s\, t\, H_{ex} \cos(\theta) \qquad (4.4)$$

Multi-domain Mono-domain

Figure 3.6 multi-magnetic domains behavior Vs the mono-domain behavior

With $H_{ex}$ is the exchange field that is created between the ferromagnetic layer and the antiferromagnetic layer. By minimizing the energy, we can find the minimum energy of the system and then the corresponding magnetization angle $\theta$. Using this description, it is possible to simulate the behavior of the active layer of the sensor (FM layer) to find the different physical parameters of the sensor such as the exchange field, the anisotropy field, the angle between the axis of easy magnetization, the magnetization of the layer and the anisotropy resistivity.

### 3.2.3 Description of the experiment:

The objective of this experiment is to study the behavior of the sensor as a function of the temperature. The first step of the experiment starts by fixating the sensor in a Linkam (LTS 420) device to isolate the sensor from all external effects (such as temperature, pressure…etc.). This device allows to control the temperature of the sensor between 77 K and 693 K with maximum heating rate of this device is 40 K/min.

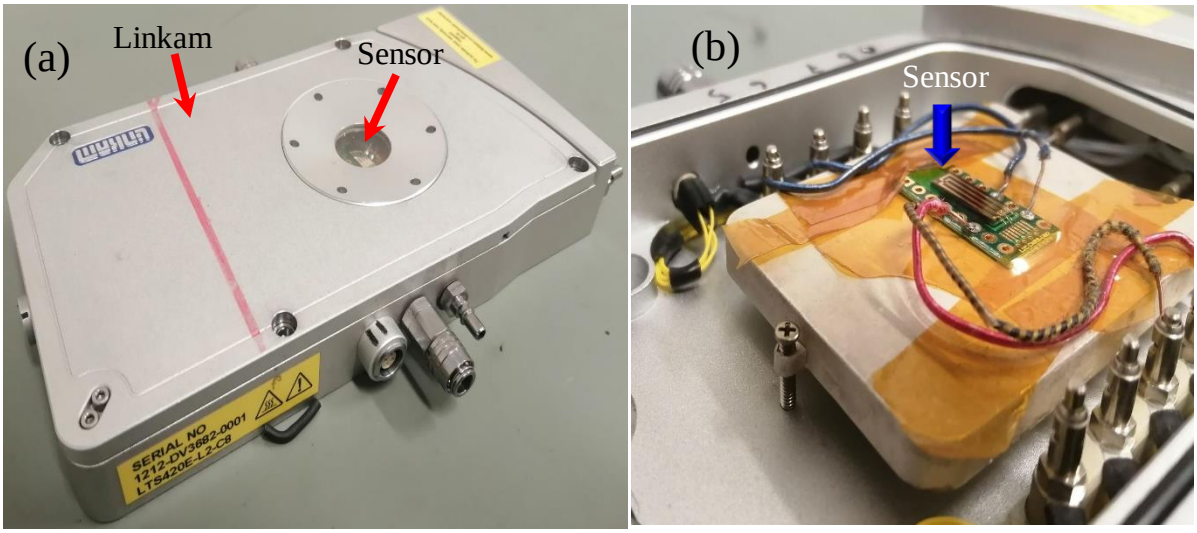


Figure 3.7 a) The Linkam device b) the Planar Hall magnetoresistance sensor placed on the Linkam device.

After the fixation of the sensor in the Linkam, the temperature was reduced by the injection of liquid nitrogen in the Linkam device (See FIG.4.7). Using the Linksys32 device, the flow of nitrogen is controlled; consequently, the temperature of the sensor is controlled. Therefore, using the nitrogen liquid, the temperature of the sensor is reduced to 110 K. In addition, the Linkam is fixed in the middle of a magnetic coil in a way where the magnetic field is applied perpendicularly (or parallel) to the easy axis of the sensor. Using the magnetic coil (See the FIG.4.8), we applied an external magnetic field between -20 mT and 20 mT to study the behavior of the sensor under the effect of this range of magnetic field.

Moreover, by using a wave function generator, we applied an electrical current of 20 mA along the easy axis of the sensor. The choice of applying the current instead of the difference in voltage is due to the fact that the change in temperature leads to a change in the resistance of the sensor which means that the current in the sensor changes with temperature change. The electrical response of the sensor (Planar Hall voltage) under the effect of the external magnetic field is measured by using a Lock-in electronic device.

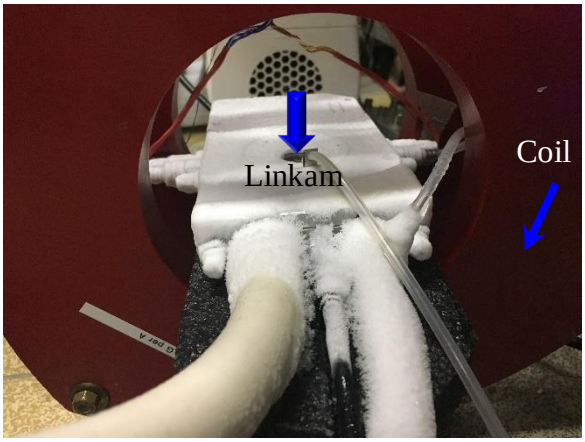


Figure 3.8 The Linkam placed in the middle of the magnetic coil.

The different devices of this experiment (the lock in and the BOP) are controlled using Python language through GPIB. Furthermore, the flow of nitrogen is controlled using the Linkam software. The temperature of the sensor is changed from 110 K to 360 K, and the rate of the increase is 20 K. For each temperature, we studied the behavior of the sensor under the effect of the external magnetic field parallel and perpendicularly to the easy axis of the sensor.

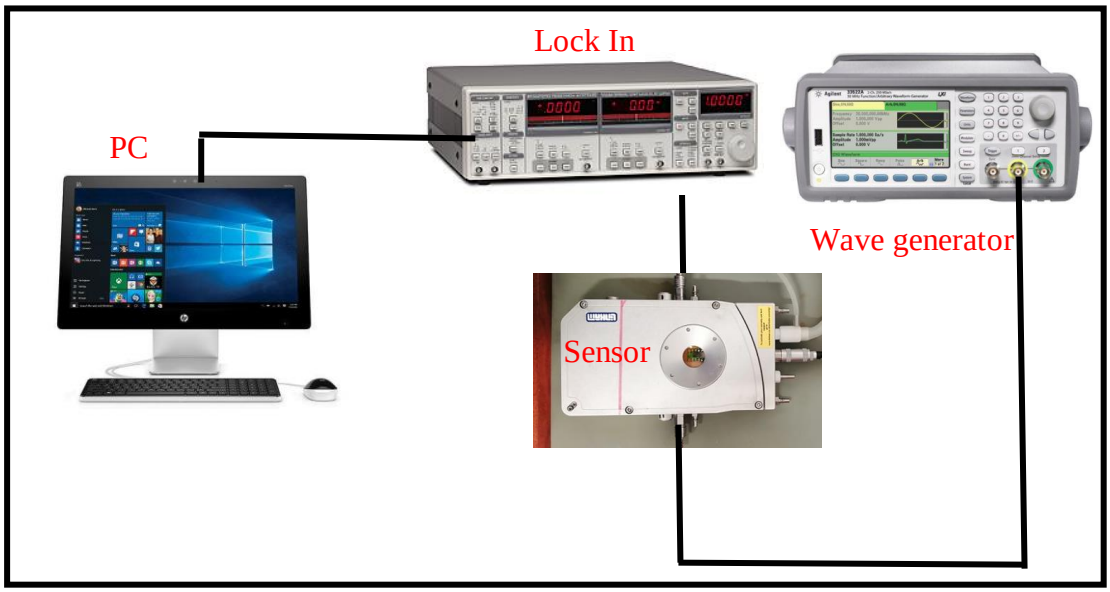


Figure 3.9 the different devices used in this experiment.

### 3.2.4 The results and dissection:

#### *3.2.4.1 The thermal stabilization of the PHE sensor:*

To understand the behavior of the Planar Hall magnetoresistance sensor under the effect of temperature, we applied an external magnetic field in the direction of the hard axis (perpendicular to the easy axis of the sensor). Most applications of the sensor rely on the application of the magnetic field perpendicular to the sensor (except for some applications that change the direction of the external magnetic field to increase the sensitivity of the sensor (see reference [60] and [61]). We changed the magnetic field's strength from -20 mT to 20 mT. Under the effect of this magnetic field, the Planar Hall voltage changes with the change of the external magnetic field with two different behaviors as shown in the figure 4.10. First, when the absolute values of the magnetic field are smaller than the extremum field, the Planar Hall voltage increases linearly with the increase of the applied magnetic field (the linearity of the Planar Hall voltage at a small magnetic field is an important propriety in the applications aimed to detect small magnetic fields). Second, when the absolute values of the magnetic field exceed the values of the extremum field, the Planar Hall voltage decreases with the increase of the magnetic field. This electrical response is due to a coherent rotation of the magnetic domain of the ferromagnetic layer. The relation between the electrical response and the direction of the magnetic domain is given by:

$$V_{\mathrm{PHE}} = \frac{I(\rho_{//} - \rho_{\perp})}{t}\cos(\theta)\sin(\theta) \qquad (4.5)$$

Where:

$I$ is the current applied to the sensor junction.

$t$ is the thickness of the ferromagnetic layer.

$\rho_{//}$ and $\rho_{\perp}$ are the longitudinal and transverse components of the thin film resistivity.

$\theta$ is the angle between the magnetization and the current direction which corresponds to the easy axis of the sensor stack. $\theta$ is a function of the direction and amplitude of the external magnetic field.

The coherent rotation of the ferromagnetic layer is due to the exchange bias interaction between the ferromagnetic layer and the antiferromagnetic. This coherent rotation of the magnetic domain appears clearly in the small hysteresis of the Planar Hall Voltage (the

hysteresis between the increased branch and the decreased branch of the Planar Hall voltage), which is an important parameter of the sensor that reflects the high quality of the sensor used in this study.

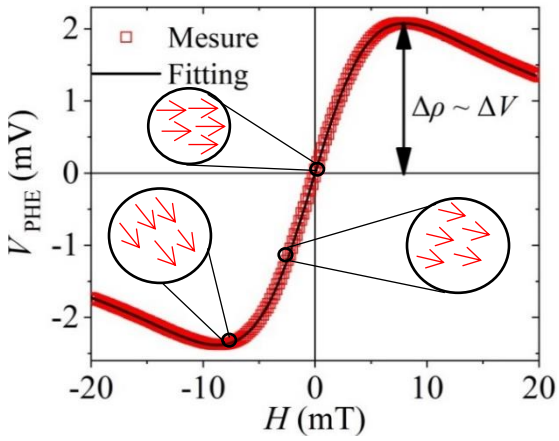


Figure 3.10 The Planar Hall voltage created from the sensor under the effect of the external magnetic field applied parallel to the hard axis of the sensor.

The calculated curve in the figure is obtained by using the Stoner-Wohlfarth model. The angle $\theta$ is calculated by the minimization of the energy of the Stoner-Wohlfarth model (See Eq. 4.4) Using the Newton-Raphson numerical method [83] based on an iterative process and replaced in the equation 4.5. As shown in the figure 4.10, the calculated curve is in good agreement with the experimental results which reflected the mono-domain behavior of the sensor when the magnetic field is applied perpendicularly to the easy axis of the sensor.

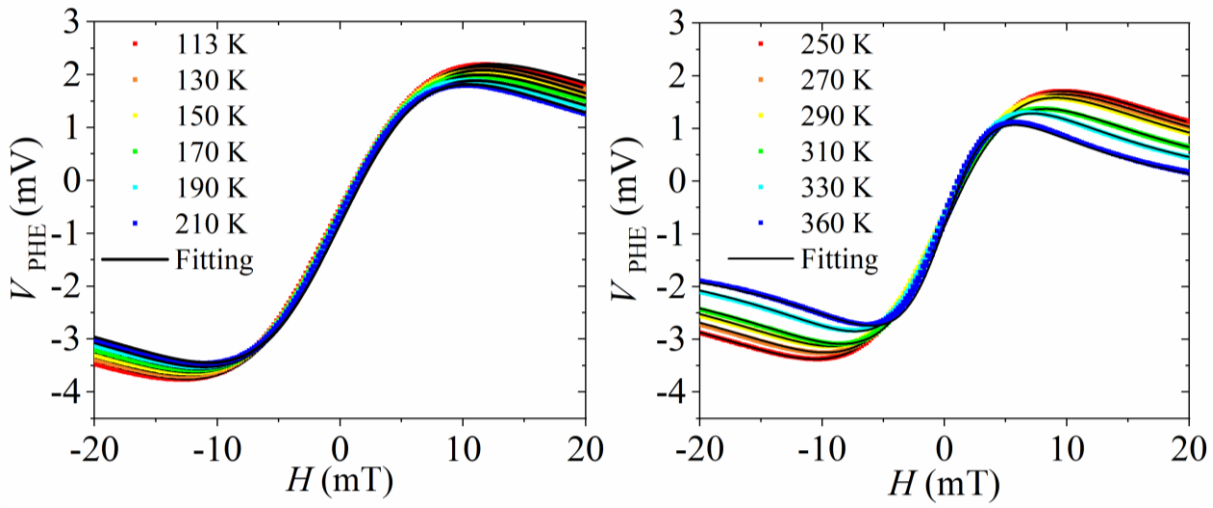


Figure 3.11 the variation of the Planar Hall voltage as a function of the external magnetic field at different temperatures from (110 K to 360 K).

FIG.4.11 shows the Planar Hall voltage variation as a function of the external magnetic field for different temperatures from 110 K (-163 °C) to 360 K (90°C). The temperature was controlled by controlling the flow of the nitrogen in the Linkam device. The rate of the temperature is 20 K (20°C). The variation of the temperature does not affect the shape of the curve of Planar Hall voltage as a function of the magnetic field. However, the increase of temperature induces a decrease of both the maximum value of the Planar Hall voltage and the value of the extremum magnetic field. This behavior is due to the decrease in the anisotropic properties of the sensor when temperature increases and the decrease of both exchange bias and coercivity fields. In addition, by dividing the values of the Planar Hall voltage as a function of the external magnetic field, we obtained the values of the sensitivity as a function of the external magnetic field. The expression of the magnetic sensitivity of the sensor is done by:

$$S(H) = \frac{I(\rho_{//} - \rho_{\perp})}{t} \cos(2\theta) \frac{d\theta}{dH} \qquad (4.6)$$

Again:

$I$ is the current applied to the sensor junction.

$t$ is the thickness of the ferromagnetic layer.

$\rho_{//}$ and $\rho_{\perp}$ are the longitudinal and transverse components of the thin film resistivity.

$\theta$ is the angle between the magnetization and the current direction.

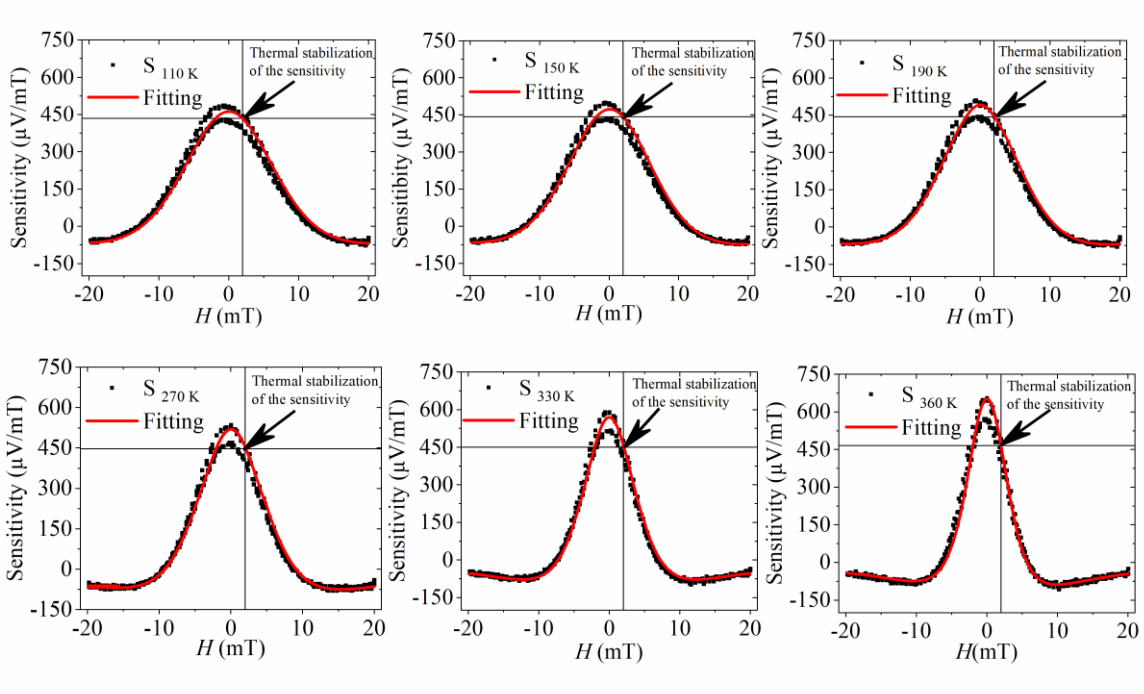

Figure 3.12 the field sensitivity of a Planar Hall sensor as a function of the external magnetic field in the temperature range from 110 K to 360 K for α = 90°.

FIG.4.12 shows the variation of the Planar Hall sensor's sensitivity as a function of the external magnetic field. The theoretical curves are calculated by using the equation 4.5, and angle $\theta$ is found by minimizing the equation of the energy.

FIG.4. 13 a) shows the calculation curves of the sensitivity of the magnetic sensor as a function of the external magnetic field for different temperatures (110 K (-160 °C), 150 K (-160 °C), 190 K (-160 °C), 270 K (-160 °C), 330 K (-160 °C), 360 K (-160 °C)). As a function of the external magnetic field, the sensitivity shows a Gaussian behavior at low field where its maximum values are obtained at $H$ = 0 mT. Furthermore, as a function of temperature, the sensitivity shows three different behaviors. First, the sensitivity increases when temperature increases if the magnetic field is between – 2 mT and 2 mT. Second, the sensitivity decreases with the increase of the magnetic field when the magnetic field is in the range [-20 to – 1.9 mT] or [+2.1 mT to 20 mT]. Third, the sensitivity is stable as a function of temperature when the magnetic field is in the range [-2.1 mT, -1.9 mT] or [1.9 mT, 2.1 mT] (which mean around -2 mT and 2 mT). FIG.4. (13) b) shows the variation of the difference between the sensitivity of the Planar Hall sensor at 110 K and the sensitivity of the Planar Hall sensor at 360 K. Again, we can see clearly that the difference between these two sensitivities is 0 when the magnetic field is equal to -2 mT or + 2 mT. Consequently, sensitivity shows high thermal stability around $H$ = ±2 mT.

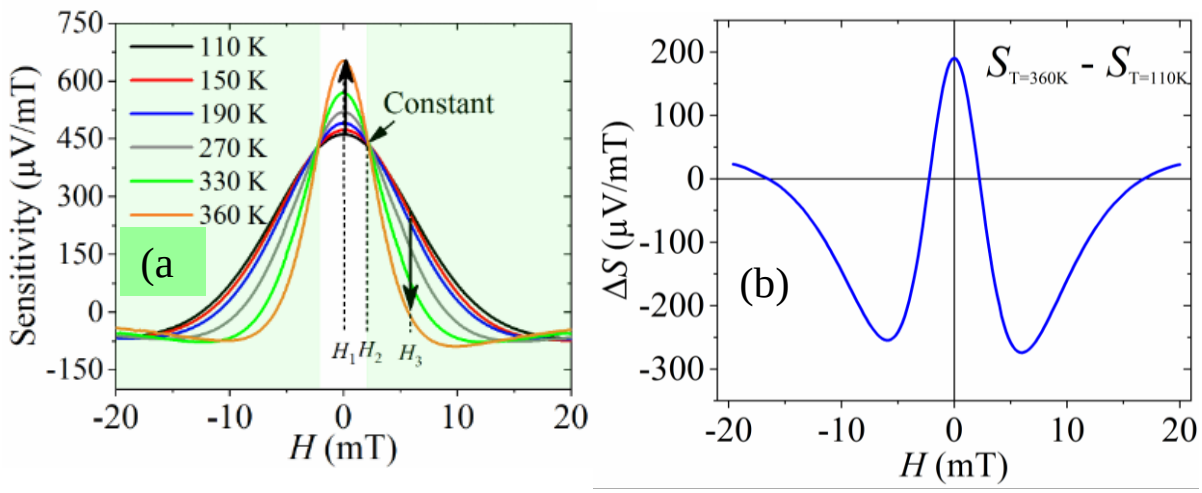


Figure 3.13 a) the variation of the sensitivity as a function of the applied magnetic field for different temperatures. b) The variation of the difference between sensitivity at 360 K and 110 K.

To compare the thermal stabilization of our method to the previous studies, we calculated the temperature coefficient of our magnetoresistance sensor's sensitivity when the magnetic field is applied around 2 mT as follows:

$$\frac{dS}{dT}_{H=2mT} = \frac{S_{360} - S_{110}}{\Delta T} = \frac{467 - 444}{250} = 90 \frac{\text{nV}}{\text{mT K}}$$

$$T_C = \frac{dS}{T_{\text{MAX}} dT}_{H=2mT} = 0.019\%/K$$

This small value of the temperature coefficient reflected the high stability of sensitivity around $H$ = 2 mT. This thermal stability of the sensor is higher than that previously achieved in the Planar Hall sensor [37], anisotropic magnetoresistance sensor [74], and giant magnetoresistance sensor. Note that in all the aforementioned studies, the sensitivity behavior was studied in smaller temperatures range compared to our study. Table 1 summarizes the comparison of the temperature coefficient of this method to the other methods.

| Sensor | Our method | PHE [37] | AMR [74] | GMR [73] | TMR [72] |
|---|---|---|---|---|---|
| The range of the temperature | 110 K to 360 K | 250 K to 350 K | 250 K to 350 K | 250 K to 350 K | 250 K to 350 K |
| Tc | 0.02%/K | 0.25%/K | 0.15%/K | 0.13%/K | 0.01%/K |

Table 3.1 The values of the temperature coefficient of the sensitivity for different magnetoresistance sensors.

### *3.2.4.2 The physical interpretation of the thermal stabilization of the PHE sensor*

To understand the physics behind the high thermal stability of the sensor's sensitivity we divided the expression of the sensitivity into two parts. The first part is the anisotropic resistivity which represents the electrical part of the sensitivity. The second part, is a function we call $f(\theta)$. The function $f(\theta)$ is related to both angel $\theta$ and the derived of the angle $\theta$ ($d\theta/dH$). This latter is related to all the magnetic parameters of the sensor such as the exchange bias, coercivity field, the external magnetic field and the angle between the easy axis and the external magnetic field:

$$\frac{d\theta}{dH} = \frac{(\sin(\alpha - \theta))^2}{[H_{ex}\cos(\theta) + H_c\,(\cos(\theta)^2 - \sin(\theta)^2)\sin(\alpha - \theta) + \cos(\alpha - \theta)[H_{ex}\sin(\theta) + H_c\cos(\theta)\sin(\theta)]} \quad (4.7)$$

FIG. 4.14 (a) shows the variation of the anisotropic resistivity as a function of the temperature. The anisotropic resistivity decreases from 3 nΩ m to 1.9 nΩ m when temperature changes from 110 K to 360 K. The decrease of resistivity when temperature increases is observed before in different magnetic materials such as the Permalloy, the NiMn, the NiCo, and NiCr [84]. This decrease of resistivity is due to the decrease of the magnetic proprieties of the sensor such as the exchange bias and the coercivity field when temperature increases. We will study the behavior of these two parameters in the next section.

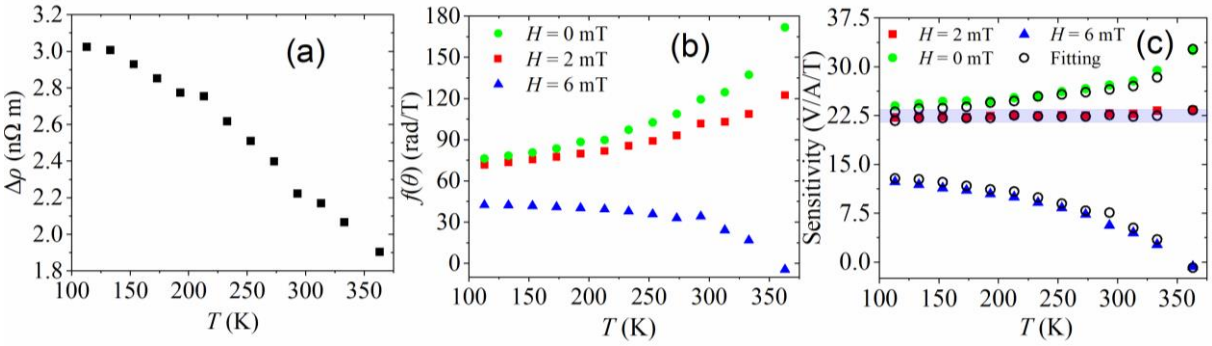


Figure 3.14 The variation of a) the anisotropic resistivity, b) function f(θ), and (c) the sensitivity as a function of the temperature.

FIG.4.14 b) shows the variation of the function $f(\theta)$ as a function of temperature for three different magnetic fields (0 mT, 2 mT and, 6 mT). For both $H$ = 2 and $H$ = 0 mT, the function $f(\theta)$ increases with the increase of temperature and for $H$ = 6 mT, the function $f(\theta)$ decreases with the increase of the temperature. By multiplying the function $f(\theta)$ by $I/2t$ and the anisotropic resistivity, we can reproduce the values of the sensitivity. FIG.4. 14 C) shows the values of the sensitivity obtained from the calculation of both functions $f(\theta)$, the anisotropic resistivity and the values obtained from the experiment results for three different fields ($H$ = 0 mT, $H$ = 2 mT and $H$ = 6 mT). The calculation values are in good agreement with experiment results. Consequently, the thermal stabilization of the sensitivity is a result of the competition between the electrical proprieties of the sensor represented by the anisotropic resistivity function and the magnetic proprieties of the sensor represented by the function $f(\theta)$ at $H$ = 2 mT.

### *3.2.4.3 The magnetization reversal of the ferromagnetic layer:*

After studying the stability of the sensitivity of the sensor as a function of temperature, we study here the magnetization reversal of the ferromagnetic layer. For this purpose, we applied the magnetic field along the easy axis' direction of the sensor and we changed the values of the magnetic field from -20 mT to 20 mT (increase branch) and from 20 mT to -20 mT

(decrease branch). FIG. 4. 15 shows the variation of the Planar Hall voltage under the effect of the external magnetic field applied parallel to the easy axis.

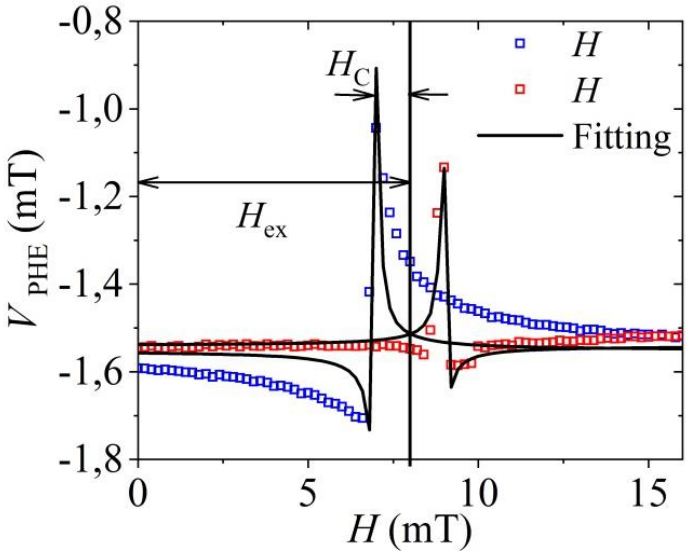


Figure 3.15 the variation of the planar hall voltage as a function of the external magnetic field applied parallel to the easy axis of the sensor.

When the external magnetic field is smaller than the exchange bias field, the exchange interaction between the ferromagnetic layer and the antiferromagnetic layer pins the magnetic moments of the ferromagnetic layer (the magnetic domain or the magnetization) in the direction of the easy axis. This reflects the stabilization of the electrical response of the sensor. At an external magnetic field around the exchange bias field, the magnetic domain is divided into small irregular magnetic domains and have no preferred direction. This behavior induces a peak in the electrical response of the sensor. Upon further increase in the magnetic field induce the reversal of the magnetic domains to the direction of the external magnetic field. Consequently, the electrical response returns to stability state. When the magnetic field decreases, the magnetic domain has the same behavior. The hysteresis appears between the two peaks (decrease branch and the increased branch of the Planar Hall voltage) is a characteristic of the coercivity phenomenon which is induced by the contribution of domain wall motion in the magnetization reversal. This hysteresis shifts along the magnetic field axis which is a characteristic of the exchange bias phenomenon. Also, we observe that the increasing and decreasing branch of the electrical response of the sensor are symmetric. This confirms that the

magnetic field is applied carefully in the direction of the easy axis. We will discuss this point further in the next sections. Using Stoner-Wohlfarth model, we can simulate the behavior of the electrical response of the sensor as shown in FIG.4. 15. The calculation curve obtained using the Stoner-Wohlfarth model is in good agreement to the experimental results.

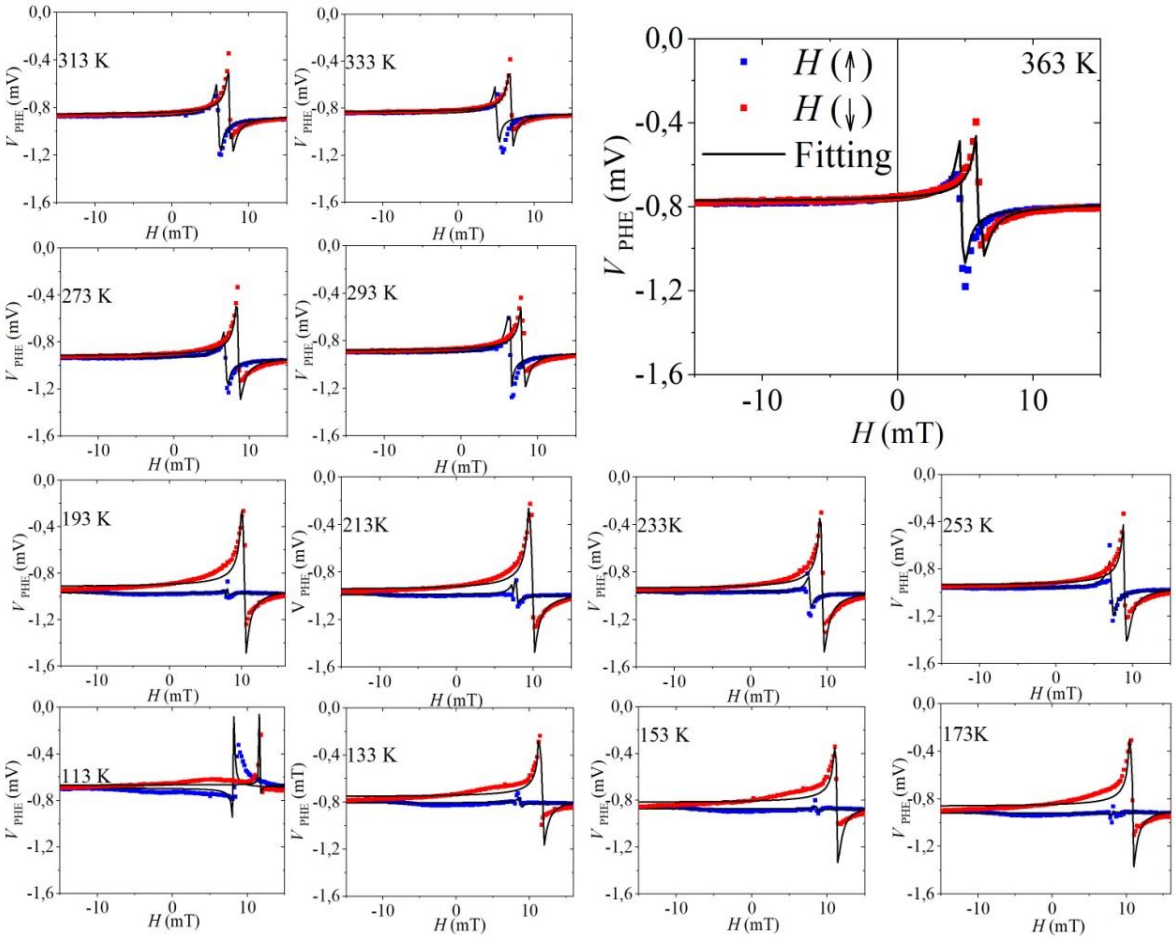


Figure 3.16 the variation of the planar hall voltage as a function of the external magnetic field for different temperatures.

FIG.4. 16 shows the variation of the Planar Hall voltage as a function of the external magnetic field for different temperatures. When temperature increases, the hysterics loop of the Planar Hall voltage shifts along the field axis to zero value due to the decrease of the exchange interaction between the ferromagnetic and the antiferromagnetic layers. The width of the hysteresis decreases with the increase of temperature due to the decrease of the coercivity field of the ferromagnetic layer. Furthermore, the decreasing and the increasing branch of the loop are symmetric at low temperatures and asymmetric at high temperatures. This shift from the symmetric behavior to the asymmetric behavior is due to a small change in the easy axis angle

from its original direction. The slight change in the easy axis could affect the magnetization reversal of the ferromagnetic materials. J. P. King and his colleagues observed a small change in the behavior of the magnetization reversal in the-NiFe/IrMn structure when the temperature changes [75]. Due to the limitation of the sensitivity of the measurement device, this change is considered as an error of measurement. Here, we prove the existence of small change in the easy axis' directions when the temperature changes. This change which affects the magnetization reversal of the ferromagnetic layer has a great importance in our understanding of the magnetic behaviors of the exchange structures. On the other hand, the exchange structure based on the NiFe interacts with IrMn is the cornerstone of many technological applications such as hard disks, the ultra-sensitive magnetic sensors and digital memories.

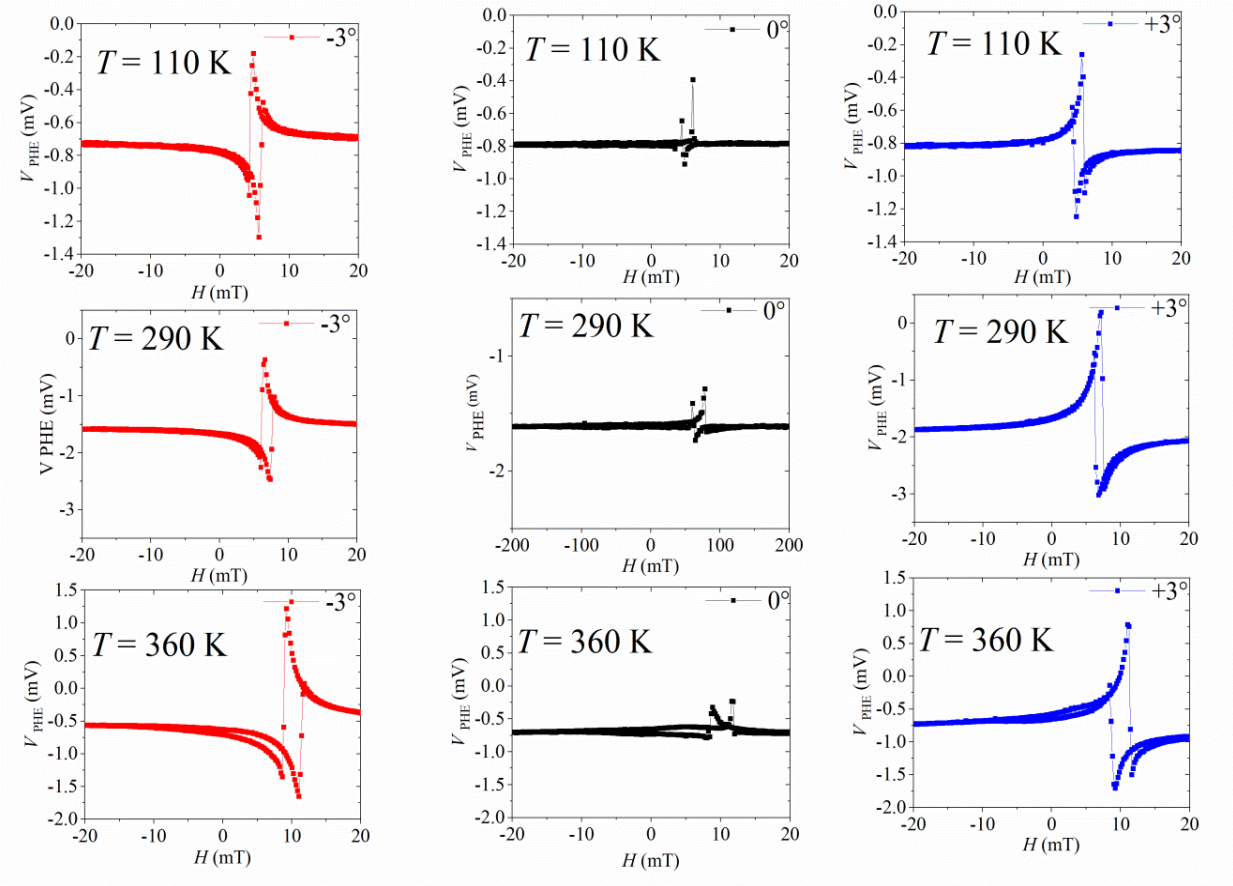


Figure 3.17 The variation of the planar Hall voltage as a function of the temperature for three different angles α = -3°, 0° and +3°, and at three different temperatures *T*= 110 K, 290 K, and 360 K.

To prove the existence of a slight change in the easy axis' direction when the temperatures change, we studied the behavior of the Planar Hall voltage for three different temperatures ( 110 K, 250 K and 360 K) and for three different angles α = 0°, α = +3° and α = -3° as shown in FIG. 4.17 The behavior of the Planar Hall voltage change from symmetrical

(See the increase and the decrease branch of the electrical response of the sensor in FIG.4.17) to asymmetrical (See the increase and the decrease branch of the electrical response of the sensor in FIG.4.17) when the easy axis angle changes from 0° to 3° or -3°. This behavior proves the observation in the previous sections. The asymmetrical behavior of the Planar Hall voltage at high temperatures is due to a change in the easy axis' direction. Note here that the small change in the easy axis' direction cannot be detected using conventional devices such as SQUID, or even the magneto-optical measurement which can detect the variation of the easy axis without quantifying it.

Combining both our measurement device and the Stoner-Wohlfarth model, we can quantify the change in the easy axis angle as a function of temperature. FIG.4.17 shows the variation of the easy axis as a function of temperature. The values of the angle α are extracted from the fitting of the experimental results. We chose two experimental conditions. In the first condition, we align the easy axis with the external magnetic field at $T$ = 110 K and we increase the temperature. The study proves that the easy axis angle changes from 0° to 1.7 °. In the second condition, we align the external magnetic field with the easy axis at $T$ = 250 K. we observed the same behavior in which the easy axis angle changes from -0.5° to + 1.25°. The study quantified the slight change of the easy axis in the range temperature from 110 K to 360 K. However, the FM behavior of the NiFe exists in wide range of temperature from 0 K to more than 800 K (Curie Temperature of NiFe) [85]. This means that the easy axis could be changed from its original direction at 0 K to around 6° at 800 K which affects strongly the magnetic behavior of the NiFe.

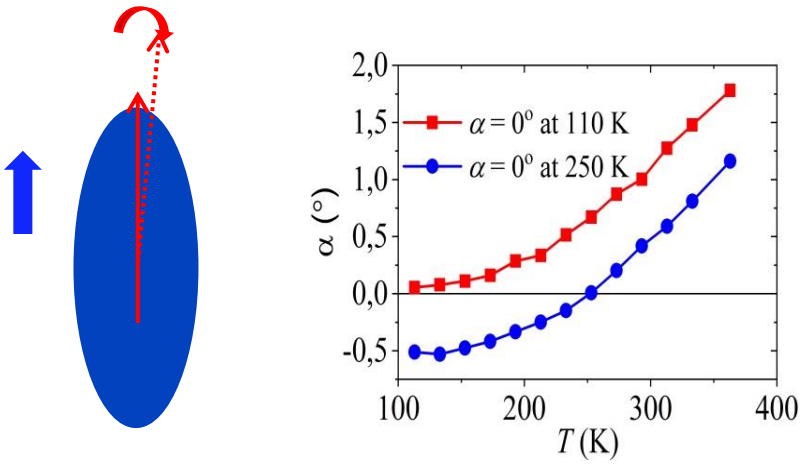


Figure 3.18 the variation of the easy axis direction as a function of the external magnetic field.

### *3.2.4.4 The effect of the change of easy axis direction on the dynamic of the magnetic domain of the ferromagnetic layer:*

When an external magnetic field is applied parallel to the easy axis, the magnetization is reversed from the direction of the easy axis to the direction of the external magnetic field through the domain wall motion. As we explained before, the magnetic domain of the ferromagnetic layer is divided into different magnetic domains with different orientation when the value of the external magnetic field approaches the value of the exchange field. The average of the magnetic angles of the different magnetic domains is the angel $\theta$. When the external magnetic field exceeds the values of the exchange bias, the angle $\theta$ changes from 0° to 180°, and when the magnetic field decreases, the angle $\theta$ changes from 180° to 360°. The behavior is reflected in the Planar Hall voltage (~ sin (2θ)) as shown in FIG.4.19. However, the small change in the easy axis' direction induces a change in the behavior of the magnetization reversal of the ferromagnetic layer. The angle θ changes from 0° to 180° when the external magnetic field exceeds the values of the exchange bias field, and return from 180° to 0° when the external magnetic field decreases. This behavior is reflected in the Planar Hall voltage (~ sin (2θ)) as shown in FIG. 4.20. The high sensitivity of the electrical response of the sensor to the direction of the easy axis allows the use of the Planar Hall measurement as a simple mechanism to study the behavior of the magnetic reversal of the ferromagnetic materials.

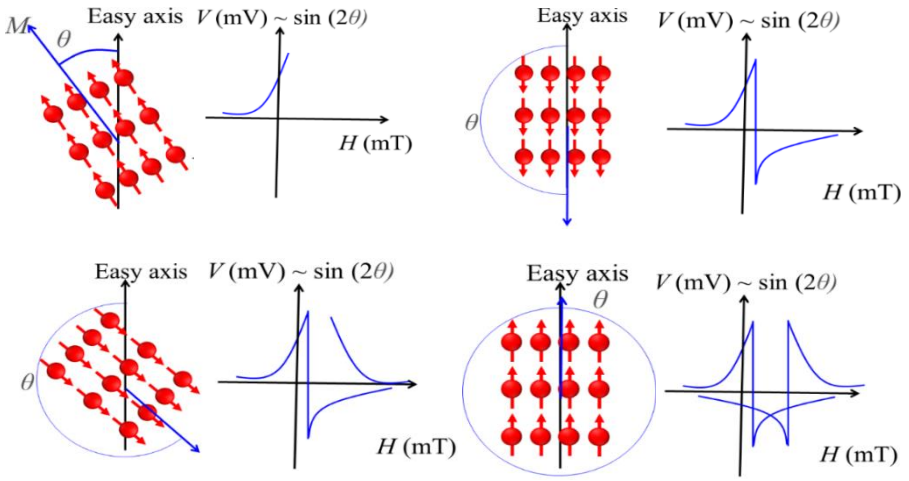


Figure 3.19 the magnetic domain behavior when the magnetic field applied parallel to the easy axis

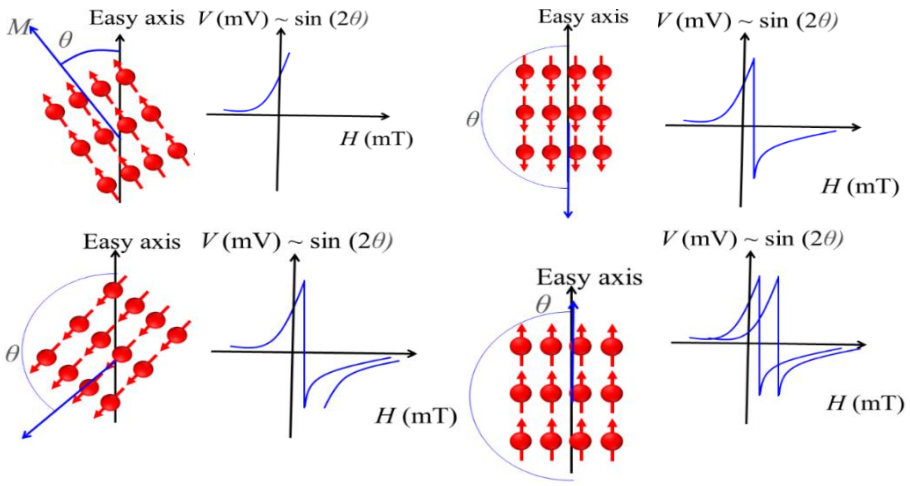


Figure 3.20 the magnetic domain behavior when the direction of the easy axis changed slightly.

Moreover, this behavior affected the magnetization reversal in the antiferromagnetic layer due to the exchange spring phenomena. A full occurs reversal of the antiferromagnetic layer from 0° to 360° when the external magnetic field aligns with the easy axis. However, the non-fully reversal occurs when the external magnetic field is not aligned to the easy axis. As shown in FIG 4.21

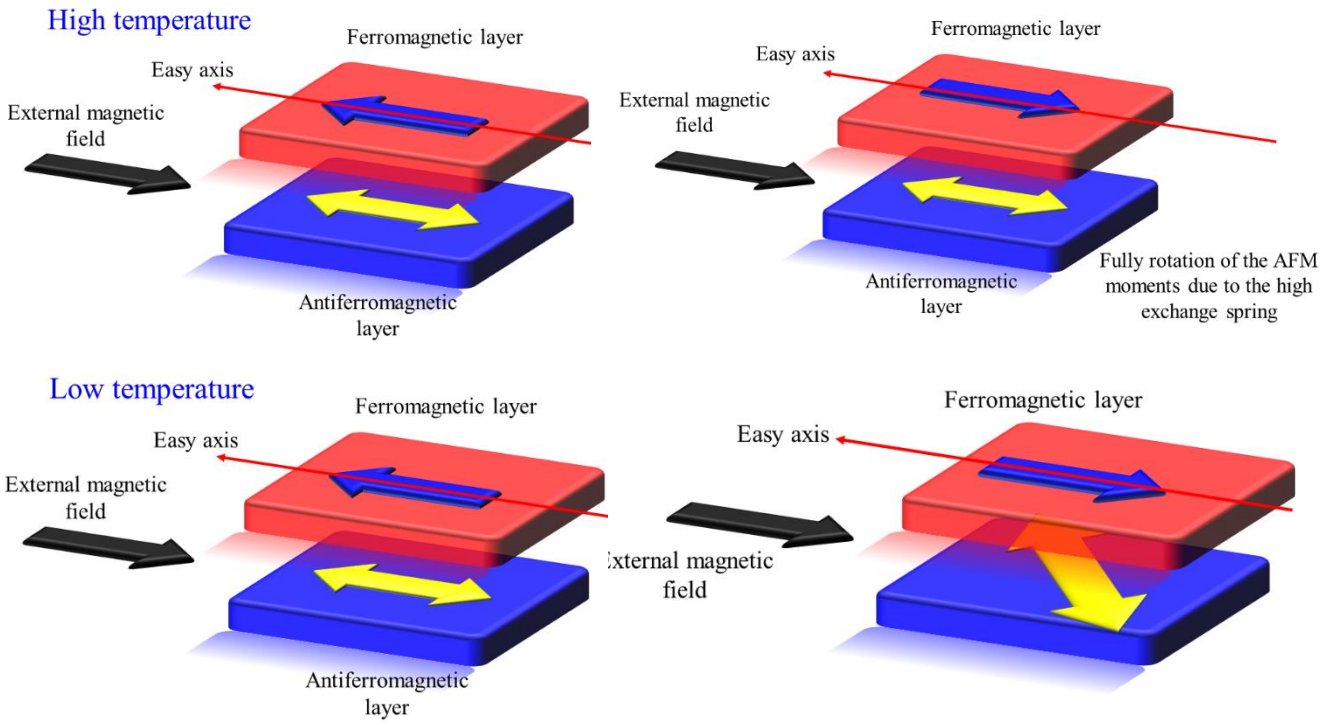


Figure 3.21 The non-full rotation of the antiferromagnetic layer when the easy axis direction changes under the effect of the temperature.

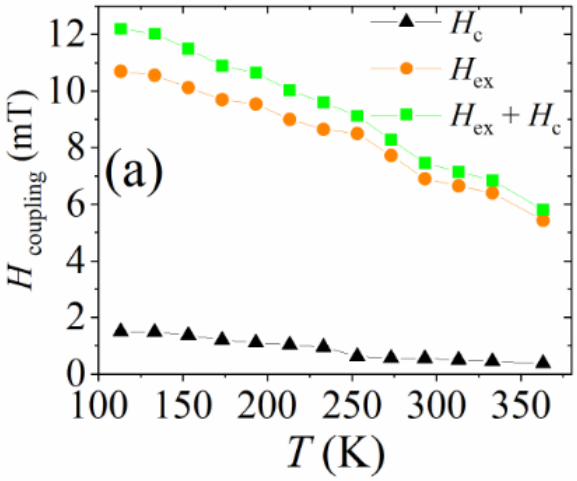


Figure 3.22 the variation of the exchange bias filed and the coercivity field as a function of the temperature.

Also we studied the behavior of the both exchange bias and coercivity field as a function of the temperature. As shown in FIG.4. 22 both the exchange bias and the coercivity field decrease when the temperature increases. The exchange bias decreases from 11 mT at 110 K to 7 mT at 360 K and the coactivity field decreases from 2 mT at 110 K to 0.2 mT at 360 K. The decrease of the exchange bias and the coercivity field when temperature increases has been observed in a wide range of FM/AFM exchange structures. At low temperatures, the high exchange interaction between the ferromagnetic moment and the antiferromagnetic moments pins the magnetic domain of the ferromagnetic layer in the direction of the easy axis which induces high values of the exchange and the coercivity fields [86]. However, at high temperatures, the high mobility of the antiferromagnetic moments allows the magnetic domain of the ferromagnetic layer to rotate easily which is reflected in low values of the exchange bias and the coercivity field [86].

FIG.4.23 shows the variation of the anisotropic energy's density as a function of the angle $\theta$ at selected temperatures ($T$ = 360K, 250K, and 110 K). Obviously, in all cases, the anisotropy energy shows two energy minima corresponding to the two easy magnetization directions of the sensor. In fact, the anisotropy energy decreases with the increase in temperature due to the weak interaction between the FM and the AFM layers. The switch of the magnetization between the two energy minima is easier at high temperature than the switch at low temperature.

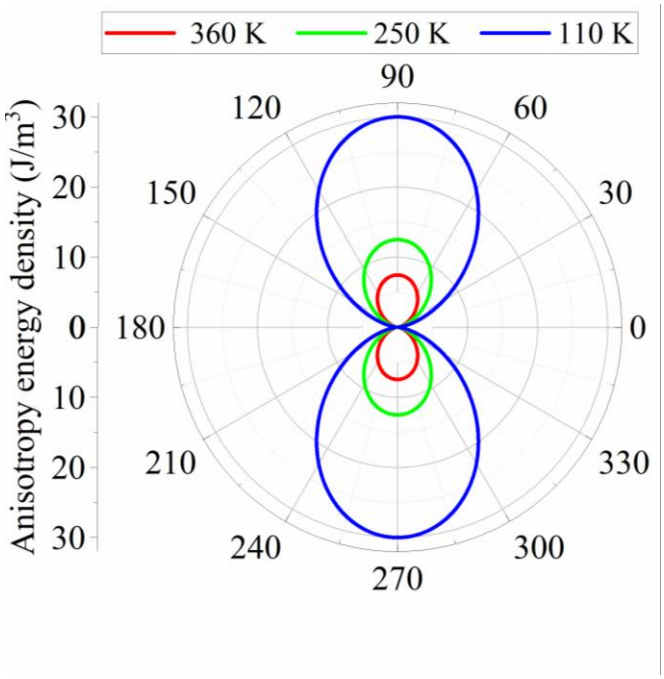


Figure 3.23 The variation of the anisotropic field as a function of the magnetization angle for three different temperatures ($T$ = 110 K, 250 K, and 360 K).

## Conclusion and perspectives:

This thesis aims to develop a high sensitivity planar Hall magnetoresistive sensor for the detection of low magnetic fields (pico-Tesla) with high accuracy. To achieve these requirements I combine both theoretical and experimental investigations. In the theoretical investigations, I first studied interactions between magnetic particles as a function of their magnetic properties, their sizes, and the distance among particles. Then the interactions of magnetic particles and a planar Hall sensor were investigated. The objective in this section is to understand the effect of the position of particles, particles' size, and the size of the sensor on the stray magnetic field of magnetic particles. I also studied the sensor's geometries to improve its particles detectivity. A rectangular geometry of sensor has been proposed to improve the detection of the particles' magnetic stray field. Effect of the presence of a monolayer and multilayers of particles on the sensor's surface was also investigated to understand the effect of ensemble particles on the sensor's surface, which reflects the reality of the particles' detection. In the last part of the theoretical study, I investigated the self-magnetic field created by the electric current passing through the sensor. In this case, both the distribution of the magnetic field on the sensor and the magnetization of the magnetic nanoparticles by this field were investigated. I determined the spatial region where the magnetic field created on the sensor has the same sign, where ever the particle is located, which optimize the detection of nanoparticles compared to the external applied magnetic field.

A new approach was proposed to increase the magnetization of nanoparticles without affecting the thermal stability of both the sensor and the nanoparticles by using a low ring conductor layer with low resistance under the planar Hall sensor' ring junction. This low resistance layer can induces a high magnetic field for magnetizing the particles locally by its high carrying current. Based on this method magnetic nanoparticles can be magnetized by a higher field (high current passing through the low resistance conductive layer) than the self-magnetic field generated by a small current passing through the active layer of sensor's junction only.

For experimental verification of highly thermal stable planar Hall sensor, firstly, I performed an experimental investigation in unstable thermal environments with two biasing cases of constant current and constant voltage. For the case of constant current biasing having high temperature dependent sensitivity, I introduced a new method to stabilize the sensor's sensitivity by the introduction of Zeeman Energy taking into account deep understanding of

physical parameters of the sensor such as the exchange bias field, the coercivity field, and the anisotropic resistivity as functions of the temperature. In the second cases with constant voltage biasing having high thermal stability of the sensitivity, I investigate the sensor's ability to withstand harsh thermal environments such as those imposed by space or industrial applications. In this part, I demonstrated the ability of the sensor to operate with high-performance levels reflected by the thermal stability of its electrical response, its low noise and also the high thermal stability of the sensitivity, which exceeds the thermal stability of other magnetoresistive sensors.

In the third part of the experimental investigations, I studied sensor’s behavior at low temperatures (from 5 K to 310 K). I proved that the sensor has a high performance levels to operate in these thermal conditions. The previous studies have allowed a deep understanding of sensor’s behavior in different thermal environments, which opened the way for wide applications of this sensor beyond current applications. Based on the minimization of the magnetic free energy, I evidenced the rotation of the easy axis of magnetization from uniaxial to biaxial anisotropy.

In the final part of my experimental studies, I characterized small amounts of gold nanoparticles by using ultra-sensitive planar Hall sensor. Based on its high sensitivity and accuracy, this new technical approach enables to detect the magnetic susceptibility of 2 µg of gold nanoparticles. The small quantities of gold nanoparticles which were characterized by this sensor cannot be characterized at room temperature using other state-of-the-art devices.

From these theoretical and experimental studies, the aim of this work is to look forward an improvement on the stability of the sensor's sensitivity in combination with the development of new geometries of a planar Hall sensor proposed theoretically to be able to characterize a nano-objets of spin-crossover nanoparticle or gold nanoparticle. This achievement is very important to reveal nanomagnetic properties governed by intermolecular interaction of a single nanoparticle without the contribution of interparticles interaction. In addition, the ability of the sensor to detect small amounts of gold nanoparticles may allow the development of ground-breaking technologies for biodetection.

On the other hand, the tendencies in manufacturing nanosatellites is pushing the development of small size magnetic sensor systems that have high thermal stability. The small size, low cost and high thermal stability of a planar Hall sensor making it a perfect candidate for nanosatellite applications. The sensor is desired to anticipate in the future for other

applications that require high thermal stability of the magnetic sensor, such as automotive, navigation, and industrial applications, especially in oil and gas sectors.

Reference:

[1] Thanh, N. T. *et al.* Thickness dependence of exchange anisotropy in NiFe/IrMn bilayers studied by Planar Hall Effect. *J. Magn. Magn. Mater.* **305**, 432–435 (2006).

[2] Oh, S. J., Le, T. T., Kim, G. W. & Kim, C. Size effect on NiFe/Cu/NiFe/IrMn spin-valve stru cture for an array of PHR sensor element. *Phys. Status Solidi A* **204**, 4075–4078 (2007).

[3] Volmer, M. & Neamtu, J. Optimisation of Spin-Valve Planar Hall Effect Sensors for Low Field Measurements. *IEEE Trans. Magn.* **48**, 1577–1580 (2012).

[4] Hung, T. Q., Jeong, J.-R., Kim, D.-Y., Duc, N. H. & Kim, C. Hybrid planar Hall-magnetoresistance sensor based on tilted cross-junction. *J. Phys. Appl. Phys.* **42**, 055007 (2009).

[5] Henriksen, A. D. *et al.* Planar Hall effect bridge magnetic field sensors. *Appl. Phys. Lett.* **97**, 013507 (2010).

[6] RIZZI, Giovanni, DUFVA, Martin, et HANSEN, Mikkel Fougt. Magnetoresistive sensors for measurements of DNA hybridization kinetics–effect of TINA modifications. *Scientific reports.* **7**, 41940 (2017).

[7] RIZZI, Giovanni, DUFVA, Martin, et HANSEN, Mikkel Fougt. Two-dimensional salt and temperature DNA denaturation analysis using a magnetoresistive sensor. *Lab on a Chip*, 2017, vol. 17, no 13, p. 2256-2263.

[8] Pham, Hong Quang, et al. Highly sensitive planar Hall magnetoresistive sensor for magnetic flux leakage pipeline inspection. *IEEE Transactions on Magnetics* **54,** 1 (2018).

[9] Hung, T. Q. *et al.* Room Temperature Magnetic Detection of Spin Switching in Nanosized Spin-Crossover Materials. *Angew. Chem. Int. Ed.* **52**, 1185–1188 (2013).

[10] Kamara, S. *et al.* Spin-Crossover Materials: Magnetic Susceptibility Study of Sub-Pico-emu Sample Using a Micromagnetometer: An Investigation through Bistable Spin-Crossover Materials. *Adv. Mater.* **29**, (2017).

[11] Cai, Y., Zhao, Y., Ding, X. & Fennelly, J. Magnetometer basics for mobile phone applications. **3** (2012).

[12] Díaz-Michelena, M. Small Magnetic Sensors for Space Applications. *Sensors* **9**, 2271–2288 (2009).

[13] Reig, C., Cubells-Beltrán, M.-D. & Ramírez Muñoz, D. Magnetic Field Sensors Based on Giant Magnetoresistance (GMR) Technology: Applications in Electrical Current Sensing. *Sensors* **9**, 7919–7942 (2009).

[14] Gaster, R. S. *et al.* Quantification of protein interactions and solution transport using high-density GMR sensor arrays. *Nat. Nanotechnol.* **6**, 314–320 (2011).

[15] Miura, Y. Hard disk drive technology: past, present and future. in *Digest of the Asia-Pacific Magnetic Recording Conference* AK1–AK1 (2002). doi:10.1109/APMRC.2002.1037621

[16] Miller, M. M., Prinz, G. A., Cheng, S.-F. & Bounnak, S. Detection of a micron-sized magnetic sphere using a ring-shaped anisotropic magnetoresistance-based sensor: A model for a magnetoresistance-based biosensor. *Appl. Phys. Lett.* **81**, 2211–2213 (2002).

[17] Zambrano, A. & Kerkhoff, H. G. A dependable AMR sensor system for automotive applications. in *2017 International Test Conference in Asia (ITC-Asia)* 59–64 (2017). doi:10.1109/ITC-ASIA.2017.8097112

[18] McFadyen, I. R., Fullerton, E. E. & Carey, M. J. State-of-the-Art Magnetic Hard Disk Drives. *MRS Bull.* **31**, 379–383 (2006).

[19] Thomson, W. XIX. On the electro-dynamic qualities of metals:—Effects of magnetization on the electric conductivity of nickel and of iron. *Proc. R. Soc. Lond.* 546–550 (1857).

[20] Smit, J. Magnetoresistance of ferromagnetic metals and alloys at low temperatures. *Physica.* **17**, 612–627 (1951).

[21] Mott, N. F. The electrical conductivity of transition metals. *Proc. R. Soc. Lond. Ser. - Math. Phys. Sci.* **153**, 699–717 (1936).

[22] McGuire, T. & Potter, R. L. Anisotropic magnetoresistance in ferromagnetic 3d alloys. *IEEE Trans. Magn.* **11**, 1018–1038 (1975).

[23] Langlinais, J. & Callaway, J. Energy bands in ferromagnetic nickel. *Phys. Rev. B* **5**, 124 (1972).

[24] Goldberg, C. & Davis, R. E. New Galvanomagnetic Effect. *Phys. Rev.* **94**, 1121–1125 (1954).

[25] Schuhl, A., Van Dau, F. N. & Childress, J. R. Low-field magnetic sensors based on the planar Hall effect. *Appl. Phys. Lett.* **66**, 2751–2753 (1995).

[26] Montaigne, F., Schuhl, A., Van Dau, F. N. & Encinas, A. Development of magnetoresistive sensors based on planar Hall effect for applications to microcompass. *Sens. Actuators Phys.* **81**, 324–327 (2000).

[27] Ejsing, L. *et al.* Planar Hall effect sensor for magnetic micro- and nanobead detection. *Appl. Phys. Lett.* **84**, 4729–4731 (2004).

[28] Thanh, N. T. *et al.* Thickness dependence of parallel and perpendicular anisotropic resistivity in Ta/NiFe/IrMn/Ta multilayer studied by anisotropic magnetoresistance and planar Hall effect. *J. Appl. Phys.* **101**, 053702 (2007).

[29] Damsgaard, C. D., Freitas, S. C., Freitas, P. P. & Hansen, M. F. Exchange-biased planar Hall effect sensor optimized for biosensor applications. *J. Appl. Phys.* **103**, 07A302 (2008).

[30] Thanh, N. T., Rao, B. P., Duc, N. H. & Kim, C. Planar Hall resistance sensor for biochip application. *Phys. Status Solidi A* **204**, 4053–4057 (2007).

[31] Hung, T. Q. *et al.* Sensitivity Dependence of the Planar Hall Effect Sensor on the Free Layer of the Spin-Valve Structure. *IEEE Trans. Magn.* **45**, 2374–2377 (2009).

[32] Hung, T. Q., Oh, S., Jeong, J.-R. & Kim, C. Spin-valve planar Hall sensor for single bead detection. *Sens. Actuators Phys.* **157**, 42–46 (2010).

[33] Thanh, N. T., Kim, K. W., Kim, C. O., Shin, K. H. & Kim, C. G. Microbeads detection using Planar Hall effect in spin-valve structure. *J. Magn. Magn. Mater.* **316**, e238–e241 (2007).

[34] Hung, T. Q. *et al.* Optimization of the Multilayer Structures for a High Field-Sensitivity Biochip Sensor Based on the Planar Hall Effect. *IEEE Trans. Magn.* **45**, 4518–4521 (2009).

[35] Hung, T. Q. *et al.* High field-sensitivity planar Hall sensor based on NiFe/Cu/IrMn trilayer structure. *J. Appl. Phys.* **107**, 09E715 (2010).

[36] Zhao, Z.-D. *et al.* The influence of ultrathin Cu interlayer in NiFe/IrMn interface on rotation of the magnetic moments. *Appl. Surf. Sci.* **332**, 710–715 (2015).

[37] Li, X.-J. *et al.* Enhanced planar hall sensitivity with better thermal stability by introducing interfacial modification of Au spacer. *J. Magn. Magn. Mater.* **381**, 386–389 (2015).

[38] Yu, G. H., Li, M. H., Teng, J., Zhu, F. W. & Lai, W. Y. Interface reactions in Ta/Ni81Fe19/Ta structures and their influence on magnetic properties. *Thin Solid Films* **484**, 208–214 (2005).

[39] Kowalewski, M. *et al.* The effect of Ta on the magnetic thickness of permalloy (Ni81Fe19) films. *J. Appl. Phys.* **87**, 5732–5734 (2000).

[40] Talantsev, A., Elzwawy, A. & Kim, C. Effect of NiFeCr seed and capping layers on exchange bias and planar Hall voltage response of NiFe/Au/IrMn trilayer structures. *J. Appl. Phys.* **123**, 173902 (2018).

[41] Pişkin, H. & Akdoğan, N. Interface-induced enhancement of sensitivity in NiFe/Pt/IrMn-based planar hall sensors with nanoTesla resolution. *Sens. Actuators Phys.* **292**, 24–29 (2019).

[42] Oh, S. J., Le, T. T., Kim, G. W. & Kim, C. Size effect on NiFe/Cu/NiFe/IrMn spin-valve structure for an array of PHR sensor element. *Phys. Status Solidi A* **204**, 4075–4078 (2007).

[43] Donolato, M. *et al.* Size-dependent effects in exchange-biased planar Hall effect sensor crosses. *J. Appl. Phys.* **109**, 064511 (2011).

[44] Damsgaard, C. D. & Hansen, M. F. Theoretical study of in-plane response of magnetic field sensor to magnetic beads in an in-plane homogeneous field. *J. Appl. Phys.* **103**, 064512 (2008).

[45] Østerberg, F. W. *et al.* Measurements of Brownian relaxation of magnetic nanobeads using planar Hall effect bridge sensors. *Biosens. Bioelectron.* **40**, 147–152 (2013).

[46] Østerberg, F. W., Rizzi, G., Henriksen, A. D. & Hansen, M. F. Planar Hall effect bridge geometries optimized for magnetic bead detection. *J. Appl. Phys.* **115**, 184505 (2014).

[47] Oh, S. *et al.* Hybrid AMR/PHR ring sensor. *Solid State Commun.* **151**, 1248–1251 (2011).

[48] Sinha, B. *et al.* Planar Hall resistance ring sensor based on NiFe/Cu/IrMn trilayer structure. *J. Appl. Phys.* **113**, 063903 (2013).

[49] Genish, I. *et al.* The effects of geometry on magnetic response of elliptical PHE sensors. *J. Appl. Phys.* **107**, 09E716 (2010).

[50] Mor, V. *et al.* Planar Hall effect sensors with shape-induced effective single domain behavior. *J. Appl. Phys.* **111**, 07E519 (2012).

[51] Grosz, A. *et al.* Planar hall effect sensors with subnanotesla resolution. *IEEE Magn. Lett.* **4**, 6500104–6500104 (2013).

[52] Grosz, A. *et al.* A high-resolution planar Hall effect magnetometer for ultra-low frequencies. *IEEE Sens. J.* **16**, 3224–3230 (2016).

[53] Hansen, T. B. G., Damsgaard, C. D., Dalslet, B. T. & Hansen, M. F. Theoretical study of in-plane response of magnetic field sensor to magnetic beads magnetized by the sensor self-field. *J. Appl. Phys.* **107**, 124511 (2010).

[54] Østerberg, F. W. *et al.* Measurements of Brownian relaxation of magnetic nanobeads using planar Hall effect bridge sensors. *Biosens. Bioelectron.* **40**, 147–152 (2013).

[55] Dalslet, B. T. *et al.* Bead magnetorelaxometry with an on-chip magnetoresistive sensor. *Lab. Chip* **11**, 296–302 (2011).

[56] Westergaard Østerberg, F., Rizzi, G. & Fougt Hansen, M. On-chip measurements of Brownian relaxation vs. concentration of 40 nm magnetic beads. *J. Appl. Phys.* **112**, 124512 (2012).

[57] Henriksen, A. D., Rizzi, G., Østerberg, F. W. & Hansen, M. F. Optimization of magnetoresistive sensor current for on-chip magnetic bead detection using the sensor self-field. *J. Magn. Magn. Mater.* **380**, 209–214 (2015).

[58] Henriksen, A. D., Rizzi, G. & Hansen, M. F. Planar Hall effect bridge sensors with NiFe/Cu/IrMn stack optimized for self-field magnetic bead detection. *J. Appl. Phys.* **119**, 093910 (2016).

[59] Henriksen, A. D., Rizzi, G. & Hansen, M. F. Planar Hall effect bridge sensors with NiFe/Cu/IrMn stack optimized for self-field magnetic bead detection. *J. Appl. Phys.* **119**, 093910 (2016).

[60] Hung, T. Q. *et al.* Planar Hall ring sensor for ultra-low magnetic moment sensing. *J. Appl. Phys.* **117**, 154505 (2015).

[61] Kim, K. W. *et al.* On-chip magnetometer for characterization of superparamagnetic nanoparticles. *Lab. Chip* **15**, 696–703 (2015).

[62] Clarke, P. J. Sputtering apparatus and method. (1977).

[63] Hanson, D. A. A. A. Turner, American photolithographer. *Hist. Photogr.* **10**, 193–211 (1986).

[64] Jaccodine, R. J. Surface Energy of Germanium and Silicon. *J. Electrochem. Soc.* **110**, 524–527 (1963).

[65] Park, B. G. *et al.* A spin-valve-like magnetoresistance of an antiferromagnet-based tunnel junction. *Nat. Mater.* **10**, 347–351 (2011).

[66] Henriksen, Anders Dahl, Shan Xiang Wang, and Mikkel Fougt Hansen. On the importance of sensor height variation for detection of magnetic labels by magnetoresistive sensors. *Scientific Reports* **5**, 12282 (2015).

[67] Tu, Bui Dinh, et al. Planar Hall bead array counter microchip with NiFe/IrMn bilayers. *Journal of applied Physics* **104,** 074701 (2008).

[68] Osterfeld, S. J. *et al.* Multiplex protein assays based on real-time magnetic nanotag sensing. *Proc. Natl. Acad. Sci. U. S. A.* **105**, 20637–20640 (2008).

[69] Kapser, K., Weinberger, M., Granig, W. & Slama, P. GMR Sensors in Automotive Applications. in *Giant Magnetoresistance (GMR) Sensors: From Basis to State-of-the-Art Applications* (eds. Reig, C., Cardoso, S. & Mukhopadhyay, S. C.) 133–156 (Springer Berlin Heidelberg, 2013). doi:10.1007/978-3-642-37172-1_6

[70] Caruso, M. J. Applications of Magnetoresistive Sensors in Navigation Systems. (1997). doi:10.4271/970602

[71] Damsgaard, C. D., Dalslet, B. T., Freitas, S. C., Freitas, P. P. & Hansen, M. F. Temperature effects in exchange-biased planar hall sensors for bioapplications. *Sens. Actuators Phys.* **156**, 103–108 (2009).

[72] Malinowski, G., Hehn, M., Montaigne, F., Jouguelet, E. & Schuhl, A. Intrinsic thermally compensated field sensor based on single magnetic tunnel junctions. *Appl. Phys. Lett.* **84**, 1204–1206 (2004).

[73] Cubells-Beltran, M. D., Reig, C., Munoz, D. R., Freitas, S. I. P. C. de & Freitas, P. J. P. de. Full Wheatstone Bridge Spin-Valve Based Sensors for IC Currents Monitoring. *IEEE Sens. J.* **9**, 1756–1762 (2009).

[74] Vopalensky, M. & Platil, A. Temperature Drift of Offset and Sensitivity in Full-Bridge Magnetoresistive Sensors. *IEEE Trans. Magn.* **49**, 136–139 (2013).

[75] King, J. P., Chapman, J. N., Gillies, M. F. & Kools, J. C. S. Magnetization reversal of NiFe films exchange-biased by IrMn and FeMn. *J. Phys. Appl. Phys.* **34**, 528–538 (2001).

[76] Meiklejohn, W. H. f& Bean, C. P. New Magnetic Anisotropy. *Phys. Rev.* **102**, 1413–1414 (1956).

[77] Gökemeijer, N. J., Ambrose, T. & Chien, C. L. Long-Range Exchange Bias across a Spacer Layer. *Phys. Rev. Lett.* **79**, 4270–4273 (1997).

[78] Li, X.-J. *et al.* Effects of interfacial roughness on the planar Hall effect in NiFe/Cu/IrMn multilayers. *Appl. Phys. A* **2**, 505–509 (2015).

[79] Stoner, E. C. & Wohlfarth, E. P. A mechanism of magnetic hysteresis in heterogeneous alloys. *IEEE Trans. Magn.* **27**, 3475–3518 (1991).

[80] Sivanandam, S. N. & Deepa, S. N. *Introduction to Genetic Algorithms*. (Springer-Verlag, 2008).

[81] Laarhoven, P. J. van & Aarts, E. H. *Simulated Annealing: Theory and Applications*. (Springer Netherlands, 1987).

[82] Erdoğmuş, P. Particle Swarm Optimization with Applications. (2018).

[83] Appendix A: Newton–Raphson Method. in *Statistical Methods for Survival Data Analysis* 428–432 (John Wiley & Sons, Ltd, 2003). doi:10.1002/0471458546.

[84] Van Elst, H. C. The anisotropy in the magneto-resistance of some nickel alloys. *Physica* **25**, 708–720 (1959).

[85] Yu, P., Jin, X. F., Kudrnovský, J., Wang, D. S. & Bruno, P. Curie temperatures of fcc and bcc nickel and permalloy: Supercell and Green's function methods. *Phys. Rev. B* **77**, 054431 (2008)

[86] Martí, X. *et al.* Electrical Measurement of Antiferromagnetic Moments in Exchange-Coupled. *Phys. Rev. Lett.* **108**, 017201 (2012)

[87] Das, Shubhankar, et al. Magnetization switching of multi-state magnetic structures with current-induced torques. *Scientific reports* **8**. 15160 (2018).

[88] Das, Shubhankar, et al. Switching of multi-state magnetic structures via domain wall propagation triggered by spin-orbit torques. *Scientific reports* **9**. 20368 (2019).

[89] Liu, R., Liew, R., Zhou, J. & Xing, B. A simple and specific assay for real-time colorimetric visualization of beta-lactamase activity by using gold nanoparticles. *Angew. Chem. Int. Ed Engl.* **46**, 8799–8803 (2007).

[90] Ludwig, J. A. & Weinstein, J. N. Biomarkers in cancer staging, prognosis and treatment selection. *Nat. Rev. Cancer* **5**, 845–856 (2005).

[91] Cairns, P. Gene methylation and early detection of genitourinary cancer: the road ahead. *Nat. Rev. Cancer* **7**, 531–543 (2007).

[92] Schofield, C. L., Haines, A. H., Field, R. A. & Russell, D. A. Silver and Gold Glyconanoparticles for Colorimetric Bioassays. *Langmuir* **22**, 6707–6711 (2006).

[93] Watanabe, S., Yoshida, K., Shinkawa, K., Kumagawa, D. & Seguchi, H. Thioglucose-stabilized gold nanoparticles as a novel platform for colorimetric bioassay based on nanoparticle aggregation. *Colloids Surf. B Biointerfaces* **81**, 570–577 (2010).

[94] Narain, R. *et al.* Preparation of Biotinylated Glyconanoparticles via a Photochemical Process and Study of Their Bioconjugation to Streptavidin. *Langmuir* **23**, 12835–12841 (2007).

[95] Nakamura-Tsuruta, S., Kishimoto, Y., Nishimura, T. & Suda, Y. One-step purification of lectins from banana pulp using sugar-immobilized gold nano-particles. *J. Biochem. (Tokyo)* **143**, 833–839 (2008).

[96] Schofield, C. L. *et al.* Colorimetric detection of Ricinus communis Agglutinin 120 using optimally presented carbohydrate-stabilised gold nanoparticles. *The Analyst* **133**, 626–634 (2008).

[97] Barrientos, A. G. *et al.* Modulating glycosidase degradation and lectin recognition of gold glyconanoparticles. *Carbohydr. Res.* **344**, 1474–1478 (2009).

[98] Thygesen, M. B. Direct chemoselective synthesis of glyconanoparticles from unprotected reducing glycans and glycopeptide aldehydes. *Chem. Commun.* 6367–9 (2009).

[99] Chuang, Y.-J., Zhou, X., Pan, Z. & Turchi, C. A convenient method for synthesis of glyconanoparticles for colorimetric measuring carbohydrate-protein interactions. *Biochem. Biophys. Res. Commun.* **389**, 22–27 (2009).

[100] Otsuka, H., Akiyama, Y., Nagasaki, Y. & Kataoka, K. Quantitative and Reversible Lectin-Induced Association of Gold Nanoparticles Modified with α-Lactosyl-ω-mercapto-poly(ethylene glycol). *J. Am. Chem. Soc.* **123**, 8226–8230 (2001).

[101] Takae, S. *et al.* Ligand density effect on biorecognition by PEGylated gold nanoparticles: regulated interaction of RCA120 lectin with lactose installed to the distal end of tethered PEG strands on gold surface. *Biomacromolecules* **6**, 818–824 (2005).

[102] Dubertret, B., Calame, M., & Libchaber, A. J. Single-mismatch detection using gold-quenched fluorescent oligonucleotides. *Nature biotechnology*, **19**, 365-370 (2001).

[103] Maxwell, D. J., Taylor, J. R., & Nie, S. Self-assembled nanoparticle probes for recognition and detection of biomolecules. *Journal of the American Chemical Society*, **124**, 9606-9612 (2002).

[104] Brown, M. D., Suteewong, T., Kumar, R. S. S., D'Innocenzo, V., Petrozza, A., Lee, M. M.and Snaith, H. J. Plasmonic dye-sensitized solar cells using core− shell metal− insulator nanoparticles. *Nano letters*, 11, 438-445 (2010).

[105] Noguchi, Y., Yamamoto, M., Ishii, H., Ueda, R., Terui, T., Imazu, K., and all. Photoresponses in gold nanoparticle single-electron transistors with molecular floating gates. *Japanese Journal of Applied Physics*, 52, 110102 (2013).

[106] Donnio, B., García-Vázquez, P., Gallani, J. L., Guillon, D., & Terazzi, E. Dendronized ferromagnetic gold nanoparticles self-organized in a thermotropic cubic phase. *Advanced Materials*, 19, 3534-3539 (2007).

[107] Crespo, P., García, M. A., Pinel, E. F., Multigner, M., Alcántara, D., De La Fuente, J. M., & Hernando, A. Fe impurities weaken the ferromagnetic behavior in Au nanoparticles. *Physical review letters*, 97, 177203 (2006).

[108] Barber, D. J. & Freestone, I. C. An investigation of the origin of the colour of the lycurgus cup by analytical transmission electron microscopy. *Archaeometry* **32**, 33–45 (1990).

[109] Jiang, Y. *et al.* Colorimetric Detection of Glucose in Rat Brain Using Gold Nanoparticles. *Angew. Chem. Int. Ed.* **49**, 4800–4804 (2010).

[110] Medintz, I. L., Clapp, A. R., Mattoussi, H., Goldman, E. R., Fisher, B., & Mauro, J. M. Self-assembled nanoscale biosensors based on quantum dot FRET donors. *Nature materials*, *2*, 630 (2003).

[111] Manohar, N., Reynoso, F. J., Diagaradjane, P., Krishnan, S., & Cho, S. H. Quantitative imaging of gold nanoparticle distribution in a tumor-bearing mouse using benchtop x-ray fluorescence computed tomography. *Scientific reports*, 6, 22079 (2016).

[112] Liu, Y., Yang, M., Zhang, J., Zhi, X., Li, C., Zhang, C. et al.Human iinduced pluripotent stem cells for tumor targeted delivery of gold nanorods and enhanced photothermal therapy. *ACS nano*, 10, 2375-2385 (2016).

[113] Lee, J., Lee, Y. H., Jeong, C. B., Choi, J. S., Chang, K. S., & Yoon, M. Gold nanorods-conjugated TiO 2 nanoclusters for the synergistic combination of phototherapeutic treatments of cancer cells. *Journal of nanobiotechnology*, 16, 104 (2018).

[114] Ueno, K., Takabatake, S., Nishijima, Y., Mizeikis, V., Yokota, Y., & Misawa, H. Nanogap-assisted surface plasmon nanolithography. *The Journal of Physical Chemistry Letters*, 1, 657-662 (2010).

[115] Suematsu, K., Watanabe, K., Tou, A., Sun, Y., and Shimanoe, K. Ultraselective toluene-gas sensor: Nanosized gold loaded on zinc oxide nanoparticles. *Analytical chemistry*, 90, 1959-1966 (2018).

[116] Corma, A., & Garcia, H. Supported gold nanoparticles as catalysts for organic reactions. *Chemical Society Reviews*, 37, 2096-2126 (2008).

[117] Depardieu, M., Demir-Cakan, R., Sanchez, C., Birot, M., Deleuze, H., Morcrette, M., & Backov, R. On the effect of gold nanoparticles loading within carbonaceous macro-mesocellular foams toward lithium-sulfur battery performances. *Solid State Sciences*, *55*, 112-120 (2016).

[118] Suber, L., Fiorani, D., Scavia, G., Imperatori, P, et al. Plunkett, W. R. Permanent magnetism in dithiol-capped silver nanoparticles. *Chemistry of materials*, 19, 1509-1517 (2007).

[119] Hurd, C. M. The magnetic susceptibility of silver and gold in the range 6–300°K. *J. Phys. Chem. Solids* **27**, 1371–1374 (1966).

[120] Granja, L. P., Martínez, E. D., Troiani, H., Sanchez, C., & Soler Illia, G. J. Magnetic Gold Confined in Ordered Mesoporous Titania Thin Films: A Noble Approach for Magnetic Devices. *ACS Applied Materials & Interfaces*, *9*(1), 965-971 (2017).

[121] Hori, H., Teranishi, T., Nakae, Y., Seino, Y., Miyake, M., & Yamada, S. Anomalous magnetic polarization effect of Pd and Au nano-particles. *Physics Letters A*, 263, 406-410 (1999).

[122] Hori, H., Yamamoto, Y., Iwamoto, T., Miura, T., Teranishi, T., & Miyake, M. Diameter dependence of ferromagnetic spin moment in Au nanocrystals. *Physical review B*, 69, 174411 (2004).

[123] He, L. Comment on "Diameter dependence of ferromagnetic spin moment in Au nanocrystals". *Physical Review B*, 81, 096401 (2004).

[124] Yamamoto, Y., Miura, T., Suzuki, M., Kawamura, N., Miyagawa, H., Nakamura, T.,et all. Direct observation of ferromagnetic spin polarization in gold nanoparticles. *Physical review letters*, 93, 116801 (2004).

[125] Dutta, P., Pal, S., Seehra, M. S., Anand, M., & Roberts, C. B. Magnetism in dodecanethiol-capped gold nanoparticles: Role of size and capping agent. *Applied physics letters*, 90, 213102 (2007).

[126] Suda, M., Kameyama, N., Ikegami, A., Suzuki, M., Kawamura, N., & Einaga, Y. Size-reduction induced ferromagnetism and photo-magnetic effects in azobenzene-thiol-passivated gold nanoparticles. *Polyhedron*, 28, 1868-1874 (2009).

[127] Michael, F., Gonzalez, C., Mujica, V., Marquez, M., & Ratner, M. A.. Size dependence of ferromagnetism in gold nanoparticles: Mean field results. *Physical Review B*, 76, 224409 (2007).

[128] Viloria, M. G., Weick, G., Weinmann, D., & Jalabert, R. A. Orbital magnetism in ensembles of gold nanoparticles. *Physical Review B*, 98, 195417 (2018).

[129] Guerrero, E., Munoz-Márquez, M. A., Fernández-Pinel, E., Crespo, P., Hernando, A., & Fernández, A. Electronic structure, magnetic properties, and microstructural analysis of thiol-functionalized Au nanoparticles: role of chemical and structural parameters in the ferromagnetic behaviour. *Journal of nanoparticle research*, *10*(1), 179-192 (2008).

[130] Gonzalez, C., Simón-Manso, Y., Marquez, M. & Mujica, V. Chemisorption-Induced Spin Symmetry Breaking in Gold Clusters and the Onset of Paramagnetism in Capped Gold Nanoparticles. *J. Phys. Chem. B* **110**, 687–691 (2006).

[131] Hernando, A. *et al.* Giant magnetic anisotropy at the nanoscale: Overcoming the superparamagnetic limit. *Phys. Rev. B* **74**, 052403 (2006).

[132] Li, C. Y., Wu, C. M., Karna, S. K., Wang, C. W., Hsu, D., Wang, C. J., & Li, W. H. Intrinsic magnetic moments of gold nanoparticles. *Physical Review B*, *83*(17), 174446 (2011).

[133] Maitra, U., Das, B., Kumar, N., Sundaresan, A., & Rao, C. N. R. Ferromagnetism exhibited by nanoparticles of noble metals. *ChemPhysChem*, 12, 2322-2327 (2011).

[134] Goettmann, F., Moores, A., Boissière, C., Le Floch, P. & Sanchez, C. A Selective Chemical Sensor Based on the Plasmonic Response of Phosphinine-Stabilized Gold Nanoparticles Hosted on Periodically Organized Mesoporous Silica Thin Layers. *Small* **1**, 636–639 (2005).

[135] Goldmann, C. *et al.* Charge Transfer at Hybrid Interfaces: Plasmonics of Aromatic Thiol-Capped Gold Nanoparticles. *ACS Nano* **9**, 7572–7582 (2015).

الملخص

يؤدي تقليص حجم المواد المغناطيسية إلى المقياس النانوي إلى ظهور خصائص جديدة. على سبيل المثال ، تُظهر جسيمات الذهب النانوية خصائص مغناطيسية غير متوقعة يمكن التحكم فيها عن طريق التحكم في الحالة الكيميائية لسطحها. تعد هذه الخصائص بتقنيات ثورية. يتطلب تطوير هذه التقنيات فهما عميقا للتفاعلات بين الجزيئات وبين الجسيمات من خلال التوصيف الدقيق لكميات صغيرة من الجسيمات النانوية (ميكرو / نانوجرام). يمثل هذا الهدف تحديًا كبيرًا نظرًا لضعف دقة الأجهزة المستخدمة حاليا. تهدف هذه الأطروحة إلى تطوير مقياس مغناطيسي دقيق عالي الحساسية يتيح الكشف عن الخصائص المغناطيسية النانوية لكمية صغيرة من الجسيمات النانوية المعزولة. لذلك ، قمنا بدراسة كيفية تحسين الاستقرار الحراري للمستشعر المغناطيسي للحصول على قياسات دقيقة في بيئة درجة حرارة غير مستقرة من 5K إلى 410 K .تم ايضا فحص التفاعلات بين الجسيمات النانوية المغناطيسية والمستشعر المغناطيسي نظريًا لزيادة قدرة المستشعرعلى الكشف عن طريق تحسين هندسته. بناء على هذه التحسينات ، أثبتت تجريبياً ان مغناطيسية كميات متناهية الصغر من الجسميات النانوية الذهبية تعزز عن طريق ربط سطحها بمواد كميائية.

## Résumé

La diminution de la taille des matériaux magnétiques jusqu'à l'échelle nanométrique conduit à l'émergence de nouvelles propriétés physique. Par exemple, les nanoparticules d'or présentent des propriétés magnétiques inattendues qui peuvent être influencées par le contrôle de l'état chimique de la surface des nanoparticules d'or. Ces propriétés promètent des technologies trés intéressantes. Pour atteindre ces objectifs, une compréhension approfondie des interactions intermoléculaires et interparticulaires grâce à une caractérisation précise de petites quantités de nanoparticules (micro / nanogrammes) est nécessaire. Cependant, cette analyse a été un défi majeur en raison de la faible résolution de détection des appareils conventionnels ($10^{-7}$ emu). Cette thèse vise ainsi à développer un micro-magnétomètre de haute sensibilité ($10^{-14}$ emu) permettant de mettre en évidence les propriétés nanomagnétiques de petites quantités de nanoparticules isolées. Par conséquent, j'ai étudié comment optimiser la stabilité thermique du capteur afin d'effectuer des mesures précises dans un environnement de température instable de 5K à 410 K. Les interactions entre les nanoparticules magnétiques et le magnétomètre ont été simulées pour maximiser la détectivité du magnétomètre en optimisant les géométries mises en jeu. J'ai pu ainsi mettre en évidence expérimentalement l'exaltation du signal magnétique d'une très faible quantité de nanoparticules d'or (2 microgrammes) fonctionnalisées « magnétisme très surprenant de l'or à l'échelle nanométrique ».



Mots de clé :

Nanomagnétisme, nanostructures, effet hall Planaire, anisotropie magnétique, Magnetoresistance, Capteurs magnétiques, susceptibilité magnétique.



## Abstract

Decrement in size of magnetic materials down to nanoscale leads to the emergence of new properties. For example, gold nanoparticles exhibit unexpected magnetic properties that can be influenced by controlling the chemical state of gold nanoparticles' surface. These properties promise attractive technologies. To reach these goal, a deep understanding of intermolecular and interparticle interactions through a precise characterization of small amounts of nanoparticles (micro/nanogrammes) is required. However, this analysis has been a major challenge due to low detection resolution of conventional devices ($10^{-7}$ emu). This thesis aims to develop a high sensitivity micro-magnetometer ($10^{-14}$ emu) enable to reveal nanomagnetic properties of small amount of isolated nanoparticles. Therefore, I study how to optimize the thermal stability of the sensor for accurate measurements in unstable temperature environment from 5K to 410 K. Interactions between magnetic nanoparticles and the magnetometer were investigated theoretically to maximize the magnetometer's detectivity by optimizing its geometries. With these improvements, I evidenced experimentally a magnetization enhancement of micrograms of gold nanoparticles by chemical functionalization.



Keywords:

Nanomagnetism, nanostructures, Planar hall effect, magnetic anisotropy, Magnetoresistance, Magnetic sensors, magnetic susceptibility.